공학박사 학위논문

Study on Heteroepitaxial Growth of Nonpolar a-plane GaN with Embedded Nano-Structures

나노 구조물이 함유된 비극성 **a**면 **GaN**의
이종에피성장에 관한 연구

2012년 8월

서울대학교 대학원
재료공학부
박 성 현

Abstract

Study on Heteroepitaxial Growth of Nonpolar a-plane GaN with Embedded Nano-Structures

Sung Hyun Park
Department of Materials Science and Engineering
The Graduate School
Seoul National University

Nitride based heterostructures grown on the (0001) polar surface substrate are affected by strong internal fields due to the spontaneous and piezoelectric polarization. These internal fields induce the spatial separation of electrons and holes in quantum wells and red-shift in emission wavelength due to the quantum confined Stark effect. To prevent these adverse effects, several groups have tried to grow GaN based structures on nonpolar or semi-polar planes. In this study, for the high efficiency nonpolar a-plane GaN light emitting diode grown on r-plane sapphire substrate, high quality a-plane GaN templates are fabricated. The study

begins with the growth of a-plane GaN buffer layer on r-plane sapphire substrate.

To obtain pit-free and improved crystal quality a-plane GaN by metal-organic chemical vapor deposition, we intentionally grew high-temperature (HT) 3-dimensional (3D) GaN buffer layers on a GaN nucleation layer. The effects of the HT 3D GaN buffer layers on crystal quality and the surface morphology of a-plane GaN were studied. The insertion of a 3D GaN buffer layer with an optimum thickness was found to be an effective method to obtain pit-free a-plane GaN with improved crystalline quality on r-plane sapphire substrates.

We utilized the 3D growth nature of a-plane GaN and controlled integration of silica nano-spheres into the rough GaN buffer layer to improve the crystalline quality of nonpolar a-plane GaN. In addition to the crystalline quality improvement by silica nano-spheres, the silica nano-spheres integrated in the GaN can improve the light extraction efficiency (LEE) of GaN-based light emitting diodes (LEDs). Nanometer-scale silica spheres act as internal scattering centers of the light emitted from the active layer of the LEDs. Thus, the angle of reflected light at the GaN/sapphire interface is distributed over a wide range of angles. Therefore, the LEE of GaN-based LEDs is increased by the enhanced probability of entering escape cone defined by the critical angle for total internal reflection. The light output power from the CIS a-plane GaN LEDs show a 130 ~ 150 % increase compared to that of the a-plane GaN LED without silica nano-

spheres in the layer. We thus attribute the improved output power for the a-plane GaN LEDs to the decreased defect density in the GaN and increased extraction efficiency of the a-plane LED fabricated with silica nano-spheres.

And, we proposed the a-plane GaN with nano-viods integrated into a-plane GaN layers using CIS process. Similar to the CIS a-plane GaN layer, integrated nano-voids in the a-plane GaN layer improved the crystalline quality of a-plane GaN subsequently grown on void due to the ELO process. In addition to the crystalline quality improvement, nanometer-scale spherical-shaped voids act as internal scattering centers of the light emitted from the active layer of the LEDs. Since the scattering of light enhanced when the refractive index difference between GaN (n=2.43) and scattering center such as silica nano-sphere (n=1.4) or nano-voids (n=1) is larger, scattering in the GaN layer will be increase by using nano-voids compared to the silica nano-spheres. Integrated nano-voids near the GaN and sapphire interface compensate the internal strain of epitaxial layers, therefore nano-voids will decrease the compressive strain in the epitaxial layer which resulted in the reduction of wafer bowing.

Keywords:

Nonpolar, a-plane GaN, r-plane sapphire, Light emitting diodes, Metal-organic chemical vapor deposition, Nano-spheres, Epitaxial

lateral overgrowth, Extraction efficiency

Student Number:

2006-23048

Contents

List of Figures

Chapter 1. Introduction

Lighting constitutes more than 20% of the total world electricity consumption, including the U.S., the European Union, and Asian countries [1]. Power generation needed for lighting contributes approximately 1900 Mt CO_2 per year (equivalent to 70% of the emissions from the world's light passenger vehicles) according to the International Energy Agency (IEA) [2]. Compared to conventional lighting technology, light emitting diodes (LEDs) lighting offers great promise as an energy-efficient, environment-friendly and affordable source of reasonably color-balanced white light owing to highly efficient LEDs. The performance of GaN-based LEDs either as direct source of light generation and or pump source for relevant dyes is front and central to general lighting applications. Over the past two decades, the performance of GaN-based LEDs has improved significantly and LEDs are now being put to use in applications such as general lighting (both indoors and outdoors), backlight for flat displays including flat panel energy efficient TVs. Among these applications, the general lighting application of the LEDs are particularly important market for GaN LEDs, and it is expected in the near future the incandescent light sources and fluorescent light sources will be all replaced by the LED-based solid state lighting. The above mentioned

applications promises an enormous market and huge economic values, and are the driving force for the ongoing research and rapid development in the area of LEDs.

The red, orange, and yellow LEDs are mainly made from AlGaInP materials system. For red LEDs, the active region is usually composed of $Ga_{0.5}In_{0.5}P$, which is lattice matched to GaAs substrates and has an energy bandgap of 1.9eV (650nm). The addition of Al to the GaInP materials can shift the emission wavelength towards shorter wavelengths (orange and yellow).

III-nitride materials have been used for producing LEDs emitting ultraviolet, violet, blue and green light sources. The main attention of this work will be focused on the GaN based LEDs. So far enormous development has been achieved for the efficiency of the GaN LEDs in the recent decades. The state-of-the-art GaN LEDs with a luminous efficacy of over 200 lm/W at room temperature have been reported [3], as compared to typically 20-30 lm/W of incandescent light bulbs and 70-90 lm/W of fluorescent light sources. However there are a few issues to address for the GaN LEDs to be widely used in general lighting, especially where high luminescence with high injection current are required. One of the issues is that the GaN-based LEDs suffer from loss of efficiency.

Wurtzite GaN-based LED structures grown along the c-axis suffer from strong polarization related to internal electric fields, which induce the spatial separation of electrons and holes in the active layers and a resulting red-shift of the emission wavelength due to the quantum confined Stark effect [4]. To prevent these adverse effects, several groups have tried to grow GaN-based LED structures on nonpolar planes, such as the a-plane or m-plane [5, 6]. To achieve high efficiency nonpolar LEDs for general illumination, the development of high quality nonpolar GaN epitaxial layers with a low defect density and a cost-effective technique to improve the light extraction efficiency of LEDs are required.

The major goal of this work is to grow high quality a-plane GaN epitaxial layer on r-plane sapphire by MOCVD and to achieve nonpolar a-plane GaN LED structure design to improve the EL efficiency. In the following sections, the background for this thesis will be presented.

1.1. GaN based light emitting diodes (LEDs) structure

General LED structures were grown on either GaN/sapphire template or bulk GaN in a vertical low-pressure metalorganic chemical vapor deposition

(MOCVD) system. As shown in Fig. 1.1, the epitaxy of a GaN LED starts with an n-type GaN which is doped with Si using SiH_4 as dopant source. It is followed by an underlayer just beneath the active region (multiple quantum wells as an example in the fig. 1.1) for improved quality. An AlGaN electron blocking layer is deposited on top of the active quantum well region to reduce the outgoing electrons from the active region. A ~100nm Mg-doped p-GaN is deposited on top of the AlGaN layer to serve as the source for hole injection. A simplified conduction band profile is shown on the right side of Fig. 1.1. After mesa etching, metallization such as Ti/Al/Ni/Au annealed at around 800 ºC for 60 seconds was used for n-type ohmic contacts and Ni/Au or indium-tin-oxide (ITO) contacts were used for the semi-transparent p-contacts. Finally, contact pads such as Ni/Au were deposited on the top of part of the mesa.

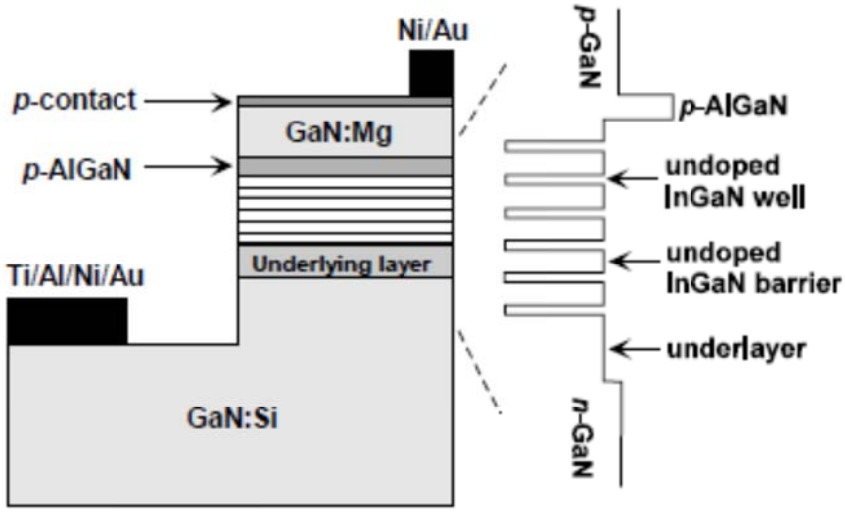

Fig 1. 1 Schematic for a typical GaN based blue LED structure with a simplified conduction band edge profile shown on the right side.

1.2. Carrier recombination in LEDs

As mentioned earlier, GaN based LEDs are composed of n-type region, active region and p-type region, etc. The electrons and holes are injected from n-side and p-side by drift-diffusion current into the active region. The recombination of electrons and holes within the active region could be radiative or non-radiative. The radiative recombination rate is described as $B\Delta n^2$, where B is the radiative recombination coefficient; Δn is the excess electron density, assuming Δn is much larger than the intrinsic carrier density since GaN is a large band-gap material and has a low intrinsic carrier density. At low injection currents, the major nonradiative recombination process is Shockley-Read-Hall (SRH), with its recombination rate described as $A\Delta n$, where A is the SRH recombination coefficient, n is the electron density. Another type of nonradiative recombination is Auger recombination, in which the energy given off by the recombination of electron and hole is used to excite another carrier to a higher energy which in turn thermalizes down to lower energy state by phonon emission. The Auger recombination rate is given by $C\Delta n^3$.

Another form of carrier loss mechanism is carrier overflow or spillover, especially for electrons as they are lighter in terms of effective mass. The electrons could escape the active region, ending up with

recombining at the p-region or the contact and not contributing to the desired emission in the active region. In order to have high internal quantum efficiency for the LEDs, both nonradiative recombination and carrier overflow or spillover should be minimized.

1.3. Nonpolar GaN for light emitting diodes

In order to achieve high efficiency for LEDs, one promising way is to use nonpolar GaN as the substrate for LEDs. Currently almost all research about GaN is about c-axis oriented wurtzite epilayers. In this kind of GaN-based heterostructures, the internal spontaneous and piezoelectronic polarization effects can cause strong electric field in the nitrides interface. Although this electric field can be advantageous for formation of two-dimensional electron gas in field-effect transistors (FETs), it can also cause spatial separation of electrons and holes in quantum wells of GaN based LEDs, thereby increasing the radiative lifetime [8] and hence reducing the quantum efficiency [9], and can also cause the red shift of LED emission (see Fig. 1. 2). This is called Quantum Confined Stark effect [10].

There are two ways to solve this polarization issue. One is to grow cubic rather than hexagonal GaN, which is nonpolar along cubic [001] direction, and therefore can avoid strong polarization-induced electric field

in heterointerfaces. Unfortunately, cubic GaN is metastable and it is also very difficult to be achieved. The other way is to grow a- or m-plane hexagonal GaN, rather than c-plane GaN. These kinds of GaN can be called nonpolar GaN, since the c axis is parallel to the substrate surface. For this kind of oriented GaN, there is no polarization-induced electric field in nitrides interfaces. Fig. 1. 3. shows schematically the m-, a-, and c-plane of GaN. These planes are perpendicular to each other.

Several groups have tried to grow GaN based structures on nonpolar a-plane $(11\bar{2}0)$ or m-plane $(1\bar{1}00)$ [11-16]. Nonpolar GaN could be obtained on various substrates, such as γ–LiAlO2 (001), a- or m-plane SiC, r- or m-plane sapphire and nonpolar GaN substrate sliced from thick c-plane GaN wafer grown by hydride vapor phase epitaxy (HVPE) [17]. Due to its relatively low cost, the $(1\bar{1}02)$ r-plane sapphire is still the most commonly used substrate for a-plane GaN growth.

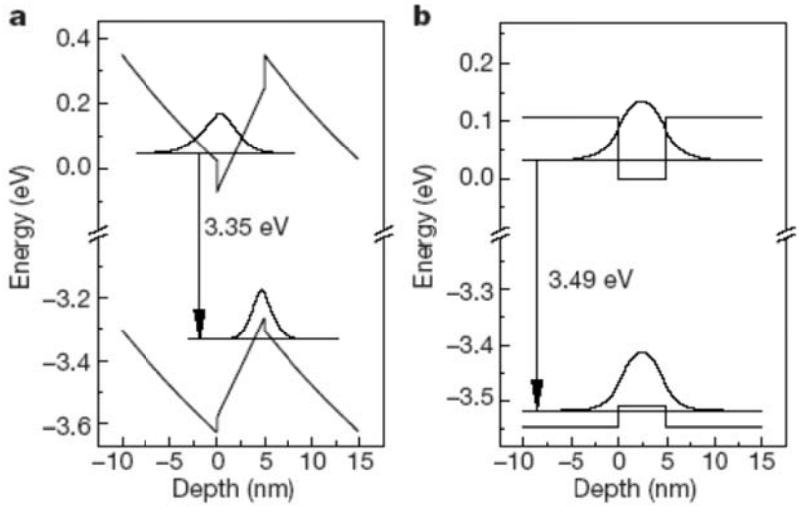

Fig 1. 2 Calculated band profiles in (5nm GaN)/(10nm $Al_{0.1}Ga_{0.9N}$) quantum wells by self-consistent effective mass Schrödinger-Poisson calculations. (a) The large electrostatic fields in the [0001] orientation result in a quantum confined Stark effect and poor electron-hole overlap. (b) The [1-100] orientation is free of electrostatic fields, thus true flat-band conditions are established [8].

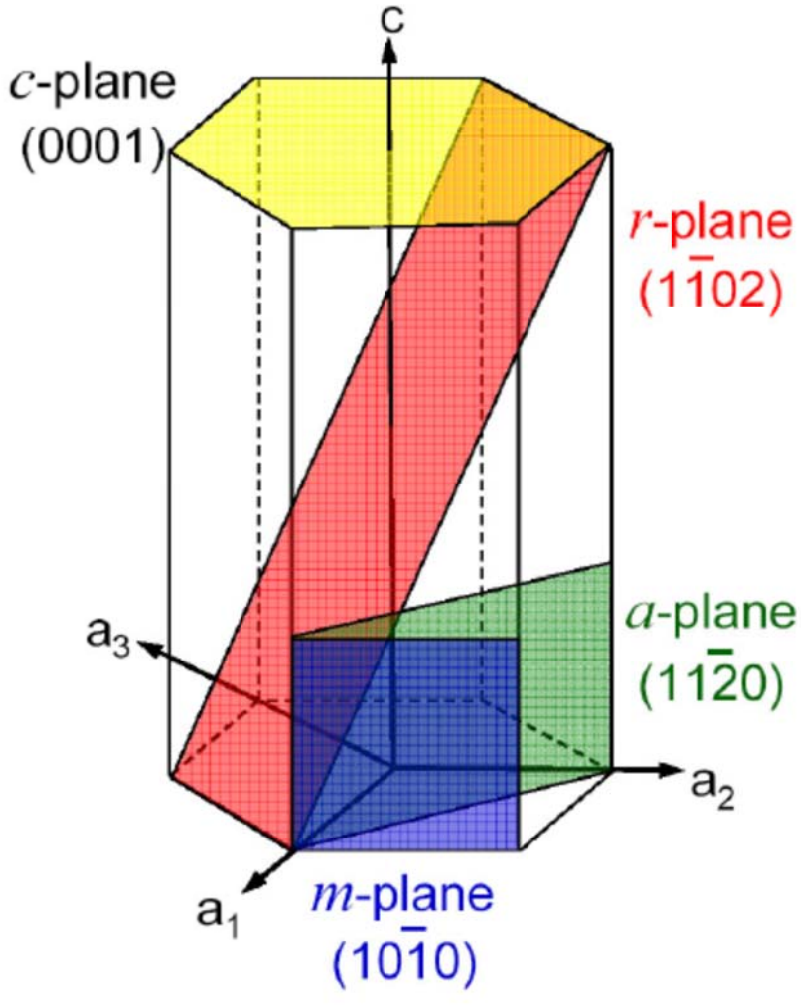

Fig 1. 3 Schematic representation of m-, a-, r- and c-plane of GaN.

1.4. Metal-organic chemical vapor deposition

MOCVD is an epitaxial growth method for preparation of semiconductor thin films based devices. The MOCVD technology has been established its ability for mass production of high-quality epitaxial layers, and has been widely used for producing nitride-based LEDs, and other compound semiconductor-based devices (such as AlInGaP-based LEDs).

The growth of epitaxial layers is typically achieved by introducing alkyls for group III, and hydrides for group V onto a heated substrate inside a vacuum chamber. For GaN system, trimethylgallium (TMGa) or triethylgallium (TEGa) is used as Ga source, and NH_3 gas is used as N source. Additionally, trimethylindium (TMIn), and trimethylaluminium (TMAl), diluted SiH_4 gases are used as In, Al, and Si (n-type dopant) sources.

The flow rate of each metalorganic (MO) source is controlled by three factors (as shown in Fig. 1. 4): MO source temperature (source temperature determines MO vapor pressure, P_{MO}) (T), carrier gas flow rate ($f_{carrier}$), and bubbler pressure ($P_{bubbler}$):

$$f_{MO}(mol/\min) = \frac{f_{carrier}(cc/\min)}{22414(cc/mol)} \cdot \frac{P_{MO}(T)}{P_{bubber} - P_{MO}(T)} \qquad [1.1]$$

where the MO source vapor pressure P_{MO} is determined by T through:

$$\log[P_{MO}] = B - A / T \qquad [1.2]$$

where A and B are constants determined empirically for each specific source.

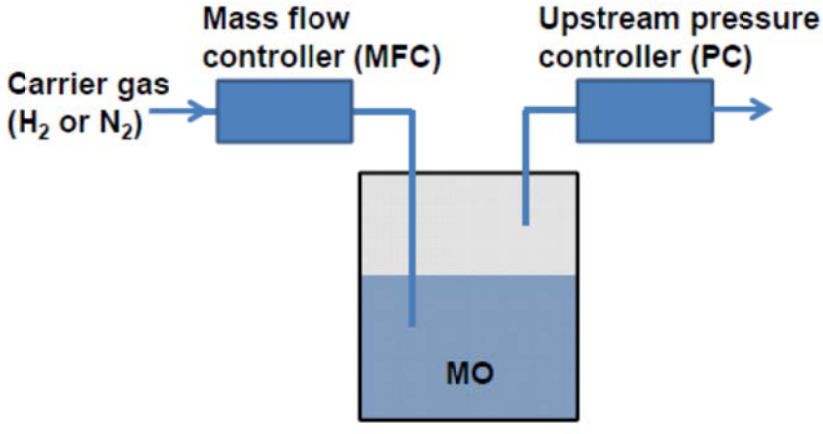

Fig 1. 4 schematic for MO source bubbler used in MOCVD system for providing MO source. The MO source mole flow rate is determined by (1) MO source temperature, (2) carrier gas flow rate, and (3) bubbler pressure (controlled by an upstream pressure controller).

1.5. Problems of heteroepitaxial nonpolar GaN

Although nonpolar GaN substrates with high crystallinity can be obtained by slicing a thick c-plane GaN wafer grown by hydride vapor phase epitaxy (HVPE),[19] r-plane sapphire is still the most commonly used large-area substrate for a-plane GaN growth, due to its relatively low cost.

However, the major drawback of r-plane sapphire substrates for the growth of nonpolar a-plane GaN is the high defect density in the a-plane GaN epitaxial layer. These defects mainly originate from the 16 % difference in the lattice constants between a-plane GaN and r-plane sapphire along the m-direction of GaN, resulting in high density, non-radiative recombination centers in a-plane GaN LEDs [18]. In addition, the enhanced in-plane growth rate anisotropy of a-plane GaN on r-plane sapphire results in the 3-dimensional (3D) growth of a-plane GaN. This 3D growth leaves a large number of micrometer-scale triangular pits on the GaN surface during the coalescence of the islands as shown in Fig. 1. 5 [18, 20, 21].

To prevent the formation of rough surfaces and/or triangular pits in a-plane GaN, most research groups have tried to grow nonpolar GaN at relatively low pressures to enhance the formation of islands in the nucleation layer [20-24]. This growth condition facilitated the coalescence of a-plane GaN at the early stage of growth, leading to pit-free surfaces. However, the

coalesced surface formed at low pressure is usually grown at the expense of numerous threading dislocations in the epitaxial layer, due to the increased number of islands formed during its growth as shown in Fig. 1.6. To improve the crystalline quality of a-plane GaN, several research groups have reported the use of conventional epitaxial lateral overgrowth (ELO) or a modified ELO process on top of low-pressure-grown a-plane GaN with high threading dislocation density [24-26].

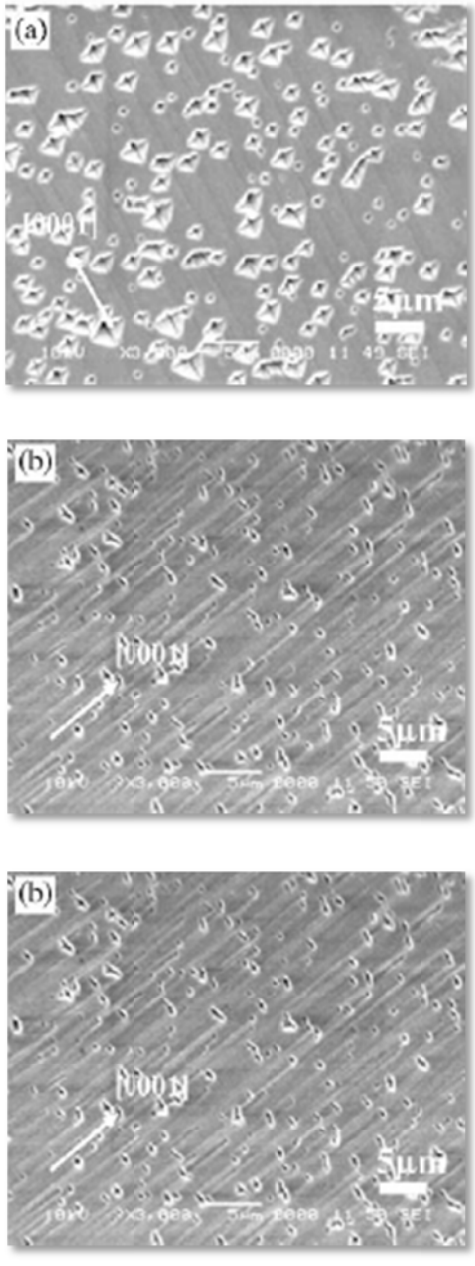

Fig 1. 5 SEM images of a-plane GaN grown under 30torr, at 1070oC, with NH3 flow rates of (a) 7060ccm, (b) 4500ccm, (c) 1000ccm, respectively [14]

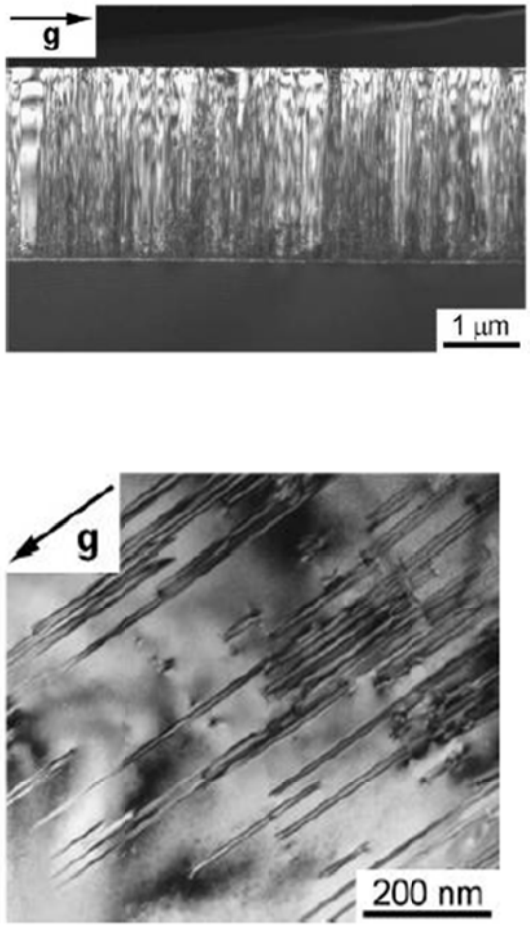

Fig 1. 6 TEM images of a-plane GaN on r-plane sapphire. (Upper) Crossectional-view for threading dislocations. (Lower) Plan-view for basal plane stacking faults [12].

1.6. Epitaxial lateral overgrowth (ELO)

In order to improve the materials properties, epitaxial lateral overgrowth (ELO) method has been used often in MOCVD system to reduce the defect density. The basic idea of this growth method is to filter out the defects by employing the dielectric masks (such as SiO_2, or SiN_x), as shown schematically in Fig. 1. 7. First, planar GaN template is grown on substrates such as sapphire, SiC or Si, which is followed by deposition of a dielectric mask by PECVD. By using standard photolithography, a set of parallel stripes is defined on the GaN template, with the separations between the dielectric stripes called "window", as shown in Fig. 1. 7(a). Then the patterned sample is loaded back into the MOCVD system for GaN regrowth. During this procedure, epitaxial growth of GaN will start in the window regions, where the microstructure of the underlying GaN template is reproduced, whereas no growth will occur above the masked area [Fig. 1. 7(b)]. The overgrown GaN will extend both vertically or laterally whose ratio highly depends on the growth conditions used. Laterally grown regions are called "wing" region, which contains much fewer defects. After certain amount of regrowth time, the overgrown GaN will get coalesced, and a few defects will be generated at the coalescence boundary [Fig. 1.7(c)]. A thorough review about this growth technique could be found in refs [27, 28].

In c-plane GaN ELO case, the stripes of dielectric films are usually aligned along the GaN m-axis $[1\bar{1}00]$ so that the laterally overgrown wings expand along the GaN a-axis $[11\bar{2}0]$, as shown in Fig. 1.7 (d). It has been demonstrated that when the mask stripes are aligned along this direction, the ratio of lateral growth rate to vertical growth rate will be higher and the sidewall facet is easier to be controlled by growth conditions [29]. In contrast, when the mask stripes are aligned along the GaN a-axis $[11\bar{2}0]$ and the lateral growth will advance along the GaN m-axis, the lateral overgrowth will be limited by a slow growth rate of $(1\bar{1}01)$ facets, which are the most stable facets in GaN and difficult to be eliminated [29]. However, in the $(11\bar{2}0)$ a-plane or $(1\bar{1}00)$ m-plane GaN ELO cases, the stripe-shaped masks should be aligned along the GaN maxis $[1\bar{1}00]$ and the GaN a-axis $[11\bar{2}0]$, so that the overgrown wings advance laterally along the GaN c-axis and result in an effective defect reduction within the overgrown GaN wing regions. The ELO technique has resulted in a significant improvement in laser diode (LD) lifetimes (>10,000 hours) at room temperature [30], but it requires extra procedure for preparing dielectric mask ex-situ, which costs time and possible sample contaminations during loading and unloading.

Another important ELO technique “nano-ELO” has been reported by Xie et al. [31], which utilizes in-situ grown porous SiNx film in MOCVD as the growth mask. However since the growth windows (i.e., nano-sized pores in SiNx film) are formed randomly during the in-situ SiNx deposition, this technique could not define the GaN lateral growth directions, which is important for an effective defect reduction in nonpolar GaN materials.

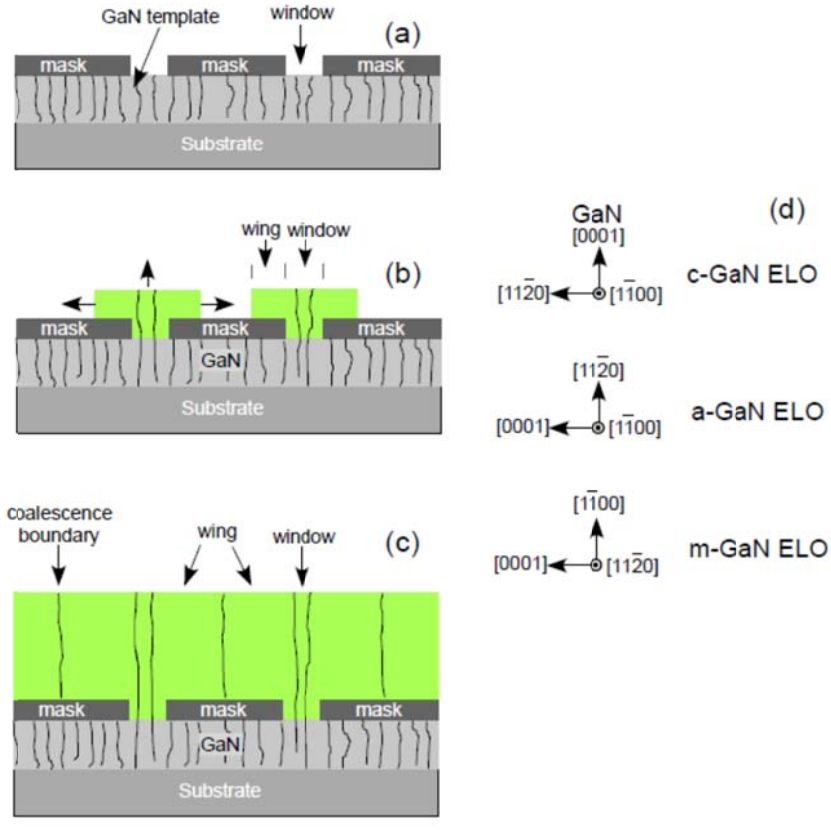

Fig 1. 7 Schematic for a conventional ELO process: (a) stripe-shaped mask (typically SiO_2 or SiNx dielectric films) on planar GaN template. (b) During regrowth step, the GaN material starts growth at the window regions, and expends both vertically and laterally. In contrast to the window regions, the overgrowth GaN above the mask regions which is normally called "wings" has very few defects. (c) the GaN wings will coalesce and form continuous films. A few defects will be generated at the coalescence boundary, where the two opposite wings coalesce. (d) The directions for the patterning of ELO mask for c-plane, a-plane and m-plane GaN ELO. [32]

1.7. Organization of this thesis

As we discussed above, the major goal of this work is to improve the quality of a-plane GaN on r-plane sapphire by MOCVD for the high efficiency nonpolar a-plane GaN light emitting diode. In chapter 2, the MOCVD system and analysis tools used in this work are introduced. So our study begins with the growth of a-plane GaN nucleation layer on r-plane sapphire substrate.

In chapter 3, to obtain pit-free and improved crystal quality a-plane GaN by metal-organic chemical vapor deposition, we intentionally grew high-temperature (HT) 3-dimensional (3D) GaN buffer layers on a GaN nucleation layer. The effects of the HT 3D GaN buffer layers on crystal quality and the surface morphology of a-plane GaN were studied.

In chapter 4 and 5, a novel, simple and inexpensive technique for improved emission efficiency of nonpolar a-plane light emitting diodes (LEDs) employing controlled integration of silica nano-spheres (CIS) is proposed. The silica nano-spheres are used as the mask layer for the regrowth of nonpolar a-plane GaN with reduced threading dislocation density and improved light extraction by the scattering process. Also, integrated silica nano-spheres reduced the polarization property of nonpolar a-plane GaN.

In chapter 6, we proposed the formation of nano-voids in a-plane GaN

layer using CIS and etching process. Similar to the CIS a-plane GaN, crystalline quality and extraction efficiency would be improved. Also, Integrated nano-voids near the GaN and sapphire interface will compensate the internal strain of epitaxial layers, therefore nano-voids will decrease the compressive strain in the epitaxial layer which resulted in the reduction of wafer bowing.

Finally conclusions and suggestions for future work will be presented in Chapter 7.

1.8. References

[1] U.S. Lighting Market Characterization, vol. I, National Lighting Inventory and Energy Consumption Estimates. Washington, D.C.: U.S. Department of Energy, 2002, Navigant Consulting, Inc. [Online].

[2] International Energy Agency, "Light's labours lost: Policies for energy-efficient lighting, in support of the G8 plan of action," 2006, p. 558.

[3] www.compoundsemiconductor.net, Vol. 16, No. 2, page 8, March (2010).

[4] D. A. B. Miller, D. S. Chemla, T. C. Damen, A. C. Gossard, W. Wiegmann, T. H. Wood and C. A. Burrus, Phys. Rev. Lett. 1984, 53, 2173.

[5] P. Waltereit, O. Brandt, A. Trampert, H. T. Grahn, J. Menniger, M. Ramsteiner, M. Reiche and K. H. Ploog, Nature 2000, 406, 865.

[6] M. D. Craven, S. H. Lim, F. Wu, J. S. Speck and S. P. DenBaars, Appl. Phys. Lett. 2002, 81, 469.

[8] R. Langer, J. Simon, V. Ortiz, N. T. Pelekanos, A. Barski, R. Andre, and M. Godlewski, Appl. Phys. Lett. 74, 3827 (1999).

[9] T. Deguchi, K. Sekiguchi, A. Nakamura, T. Sota, R. Matsuo, S. Chichibu, and S. Nakamura, Jpn. J. Appl. Phys. Part 2-Letters 38, L914 (1999).

[10] D. A. B. Miller, D. S. Chemla, Phys. Rev. Lett. 53, 2173 (1984).

[11] P. Waltereit, O. Brandt, A. Trampert, H. T. Grahn, J. Menniger, M.

Ramsteiner, M. Reiche, and K. H. Ploog, Nature 406, 865 (2000).

[12] C. Q. Chen, M. E. Gaevski, W. Sun, E. Kuokstis, J. P. Zhang, R.S. Fareed , J. Wang, G. Simin, A. Khan, H. Maruska, D. Hill, M. Chou, B. Chai , Appl. Phys. Lett. 81,3194 (2002)

[13] A. Chitnis, C. Chen, V. Adivarahan, M. Shatalov, E. Kuokstis, V. Mandavilli, J. Yang, A. Kahn, Appl. Phys. Lett. 84, 3663 (2004)

[14] M. Craven, P. Waltereit, J. Speck, S. DenBaars. Appl. Phys. Lett. 84, 496 (2004)

[15] N. Akopian, G. Bahir, D. Gershoni, M. Craven, J. Speck, S. DenBaars Appl. Phys. Lett. 86, 20 (2005)

[16] Kuokstis E, Chen C Q, Gaevski M E, Sun W H, Yang J W, Simin G, Khan M A, Muruska H P, Hill D W, Chou M C, Gallagher J J, Chai B, 2002 Appl. Phys. Lett. 81 4130

[17] K.-C. Kim, M. Schmidt, H. Sato, F. Wu, N. Fellows, M. Saito, F. Wu, N. Fellows, M. Saito, K. Fujito, J. Speck, S. Nakamura, S. DenBaars, Phys. Status Solidi (RRL) 1, 125 (2007)

[18] M. D. Craven, S. H. Lim, F. Wu, J. S. Speck and S. P. DenBaars, Appl. Phys. Lett. 2002, 81, 469.

[19] K. C. Kim, M. C. Schmidt, H. Sato, F. Wu, N. Fellows, Z. Jia, M. Saito, S. Nakamura, S. P. DenBaars and J. S. Speck, Appl. Phys. Lett. 2007,

91, 181120.

[20] X. Ni, Y. Fu, Y. T. Moon, N. Biyikli, and H. Morkoç, J. Cryst. Growth 2006, 290, 166.

[21] Q. Sun, C. D. Yerino, T. S. Ko, Y. S. Cho, I.-H. Lee, J. Han and M. E. Coltrin, J. Appl. Phys. 2008, 104, 093523.

[22] T. S. Ko, T. C. Wang, R. C. Gao, H. G Chen, G. S. Huang, T.C. Lu, H. C. Kuo, J. Cryst. Growth 2007, 300, 308.

[23] S.-N Lee, H. S. Paek, J. K. Son, T. Sakong, O. H. Nam, Y. Park , J. Cryst. Growth 2007 307, 358.

[24] F. Wu, M. D. Craven, S. H. Lim, and J. S. Speck, J. Appl. Phys. 2003, 94, 942.

[25] Q. Li, Y. Lin, J. R. Creighton, J. J. Figiel and G. T. Wang, Adv. Mater. 2009, 21, 2416.

[26] D. Iida, M. Iwaya, S. Kamiyama, H. Amano and I. Akasaki, J. Cryst. Growth 2009, 311, 2887.

[27] B. Beaumont, P. Vennégues, and P. Gibart, Physica Status Solidi (b) 227, 1 (2001).

[28] Pierre Gibart, Bernard Beaumont, Philippe Vennégues, “Epitaxial Lateral Overgrowth of GaN” in “Nitride Semiconductors - Handbook on Materials and Devices” P. Ruterana, M. Albrecht and J. Neugebauer,

Eds. Wiley 2003.142

[29] K. Hiramatsu, K. Nishiyama, A. Motogaito, H. Miyake, Y. Iyechika, and T. Maeda, Physica Status Solidi (a) 176, 535 (1999).

[30] S. Nakamura, M.Senoh, S. Nagahama, N. Iwasa, T. Yamanda, T. Matsushita, H. Kiyoku, Y. Sugimoto, T. Kozaki, H. Umemoto, M. Sano, and K. Chocho, Appl. Phys. Lett., 72, 211 (1998).

[31] J. Xie, Ü. Özgür, Y. Fu, X. Ni, H. Morkoç, C. K. Inoki, T. S. Kuan, J. V. Foreman, and H. O. Everitt, Appl. Phys. Lett. 90, 041107 (2007).

[32] X. Ni, “Growth and characterization of non-polar GaN materials and investigation of efficiency droop in InGaN light emitting diodes”, Ph. D dissertation, Virginia Commonwealth Univ. (2010)

Chapter 2. Growth and analysis tools

2.1. Growth process and LED fabrication

2.1.1. MOCVD system

In this work, Thomas Swan 3 x 2" (incorporated 3 substrates of 2 inch size) close coupled showerhead (CCS) MOCVD system was used to grow nonpolar nitride semiconductor epitaxial layers.

Trimethylgallium (TMGa, (CH3)3Ga) and Trimethylindium (TMIn, $(CH_3)_3In$) were used for group III sources. Solkatronics^{TM} Blue-Ammonia (NH3) of 99.9999 % purity was used for group V sources.

Bis(cyclopentadienyl)magnesium (Cp_2Mg, $(C_5H_5)_2Mg$) and 10 ppm diluted silane (SiH_4) was installed for p-type and n-type doping, respectively.

2.1.2. Sample preparation

r-plane sapphire is used as the substrate for the growth of a-plane GaN. At first, it was ex-situ cleaned at air. For ex-situ cleaning, sapphire wafer was immersed in acetone and methanol with ultrasonic by turns, in each turn for 10 min at 40 ^{o}C. After degreasing, wafer was rinsed in flowing de-ionized water for 10 min. Then, wafer was dried with nitrogen. After ex-situ

cleaning, wafer was loaded into the reactor, and then in-situ cleaned in hydrogen ambient at ~1100 ^{o}C.

2.1.3. Device fabrication

The a-plane GaN LED structures consist of n-type a-plane GaN, three pairs of InGaN/GaN quantum well layers (3 nm/12 nm) and p-type a-plane GaN. ITO and Ti/Al/Ti/Au were used as the p- and n-type contact materials, respectively.

2.2. Analysis tools

2.2.1. Atomic force microscopy (AFM)

The AFM measurements were performed in an atmospheric ambient to investigate surface morphology of a-plane GaN sample. The Au-coated Si probes were used in noncontact mode using Seiko SPA-400. For statistical analyses, Nanotec WSxM v4.0 was used.

2.2.2. Transmission electron microscopy (TEM)

The TEM specimens were prepared using conventional mechanical polishing followed by ion milling using a specimen stage cooled by liquid nitrogen. Some samples were prepared using focused ion beam. Bright-field and high-resolution transmission micrographs were obtained by a FEI Tecnai F20 electron microscope operated at 200 kV.

2.2.3. Photoluminescence (PL)

PL spectroscopy is a contactless, nondestructive method of probing the electronic structure of materials. PL measurements were made at room temperature. The 325 nm line of He-Cd laser was used. The PL signal was dispersed by a SPEX monochromator and detected by liquid-nitrogen-cooled

charge coupled device (CCD) detector.

2.2.4. X-ray diffraction (XRD)

Panalytical X'pert instrument and Bruker D8 Discovery were used for high resolution XRD measurement and ω-scan. The angle divergence of 12 arcsec or less can be obtained by 4 bounce Ge 022 channel cut monochromator.

2.2.5. Cathodoluminescence (CL)

Gatan Mono CL3 and 4 systems were used to investigate luminescence properties of a-plane GaN samples. The CL measurements were carried out in panchromatic or monochromatic mode at room temperature or 77 K using LN_2. The acceleration voltage was varied to investigate the dependence of the CL spectra.

Chapter 3. Growth of a-plane GaN using 3D shaped buffer layer

3.1. Introduction

The major drawback of r-plane sapphire substrates for the growth of nonpolar a-plane GaN is high density defects in the a-plane GaN epitaxial layer. These defects mainly originate from the 16% difference in lattice constants between a-plane GaN and r-plane sapphire along the m-direction of GaN, resulting in non-radiative recombination centers in a-plane GaN LEDs [9]. In addition, enhanced in-plane growth rate anisotropy of a-plane GaN on r-plane sapphire results in 3-dimensional (3D) growth of a-plane GaN [10]. The 3D growth nature leaves a large number of micrometer-scale triangular pits on the GaN surface during the coalescence of islands [1-4].

To obtain pit-free, high-quality non-polar a-plane GaN on r-plane sapphire, various nucleation layers such as low-temperature (LT) GaN [1-4], high-temperature (HT) GaN [5-7], HT AlGaN [8], LT AlN, and HT AlN [4, 9] have been used. To further improve the quality of a-plane GaN, several research groups have reported the use of multiple GaN buffer layers [2, 10].

In this research, we focused on the effects of a HT 3D GaN buffer layer on a-

plane GaN grown by using metal-organic chemical vapor deposition (MOCVD). We obtained pit-free a-plane GaN with improved crystalline quality by modifying the growth of the 3D buffer layer and successfully fabricated a-plane GaN LEDs with negligible peak shift.

3.2. Experimental procedure

The a-plane GaN layers were grown on r-plane sapphire substrates in a Thomas Swan 3 × 2 inch close-coupled showerhead MOCVD reactor. After thermal cleaning of the r-plane sapphire substrate (-0.2 ± 0.05^{o} toward the m-axis of sapphire) in a H_2 ambient for 5 min at 1100 ^{o}C, we performed nitridation in an NH_3 ambient for 5 min at the same temperature. Then, the HT GaN nucleation layers were grown for 5 min at 1040 ^{o}C at a 100 Torr of nitrogen carrier gas. Subsequently, a-plane GaN was grown at the same growth temperature with a hydrogen carrier gas to form 2.8-μm-thick GaN. Tirmethylgallium (TMGa) and ammonia (NH_3) were used as precursors. More detailed growth procedure of the a-plane GaN are reported elsewhere [7].

To evaluate the effect of HT 3D GaN buffer layer on the morphology as well as the crystal quality of a-plane GaN layer, we grew 3D buffer layers with different thicknesses were grown at 300 Torr on the GaN

nucleation layer. During the entire growth procedure, the reactor pressure was maintained at 100 Torr, except for the growth of the 3D GaN buffer layer.

3.3. Growth of a-plane GaN with 3D shaped buffer layer

Generally, the islands in the a-plane GaN nucleation layer have anisotropic shapes with a triangular base, inclined facets and a vertical facet, which is the presumably $\{1\bar{1}01\}$ and $(000\bar{1})$ plane [3-11]. At a relatively high growth pressure such as 300 Torr, the growth rate anisotropy of a-plane GaN on r-plane sapphire was enhanced [2], and these 3D islands grew to leave a large number of micrometer-scale triangular pits on the GaN surface during the coalescence of islands. To prevent the formation of rough surfaces and/or triangular pits in the a-plane GaN, most research group have tried to grow nonpolar GaN at a relatively low pressure to enhance the formation of islands in the nucleation layer [1-7]. This growth condition facilitated the coalescence of a-plane GaN at the early stage of growth, leading to pit-free surfaces. However, low-pressure growth generated many threading dislocations in the epitaxial layer at the expense of the coalesced surface due to the increased number of islands during the growth.

To overcome these drawbacks, we intentionally utilized the 3D growth nature of a-plane GaN on r-plane sapphire and optimized the thickness of the 3D GaN buffer layer to improve crystal quality and to reduce the density of triangular pits. The surface morphology of the 3D GaN buffer layer grown on a r-plane sapphire substrate was investigated by using a scanning electron microscope (SEM). Fig. 3. 1(a) and 1(b) show the plan-view and the cross-sectional-view SEM images of the 3D GaN buffer layer. The cross-sectional image is viewed along the [0001] direction of GaN. The 3D morphology will be helpful to bend threading dislocations and to obtain an improved crystal quality of the a-plane GaN layer. However, the thickness and the distribution of 3D GaN buffer layer should be optimized, because too thin a layer would not be enough to affect the dislocation movement and too thick a layer would leave triangular pits on the surface. The thickness of the 3D GaN buffer layer was varied, and the crystal qualities of fully-coalesced, pit-free 2.8-μm-thick GaN epitaxial layers were estimated by using X-ray diffraction (XRD). The nominal thickness of the 3D GaN buffer layers was estimated by using the growth rate of flat a-plane GaN layers grown under the same growth conditions.

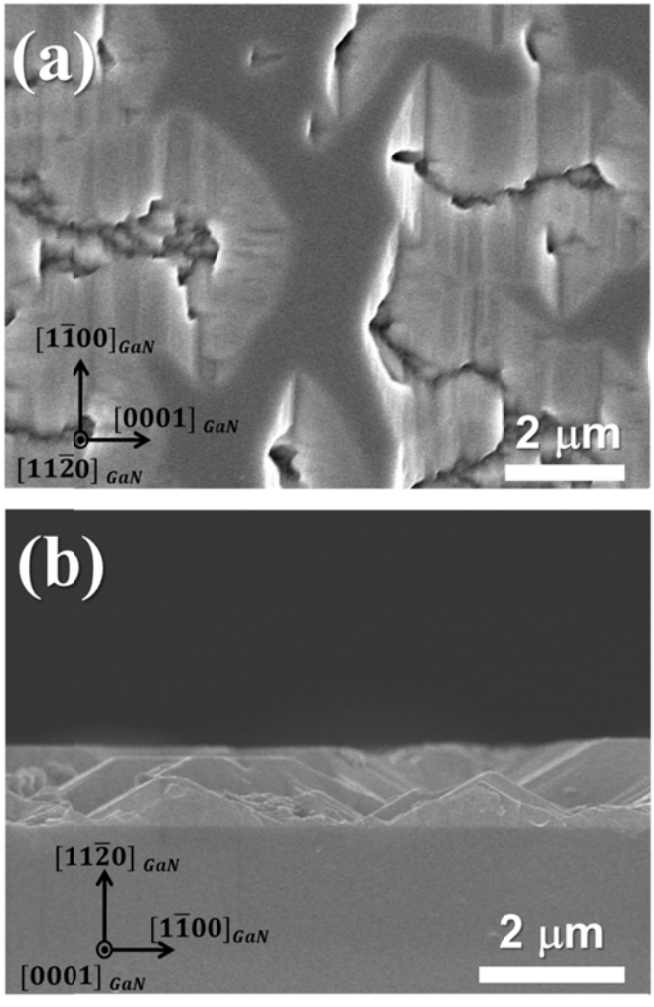

Fig. 3. 1 SEM images of a-plane 3D GaN buffer layer: (a) plan-view and (b) cross-sectional-view along the c-direction of GaN.

Fig. 3. 2 shows the results for the XRD full width at half maximums (FWHMs) at various 3D buffer layer thicknesses. As shown in Fig. 3. 2, the FWHMs along the [0001] c-axis decreased from 768 to 632 arcsec at a 600-nm buffer thickness and increased slightly afterwards. On the other hand, the FWHM along the m-axis of GaN drastically decreased from 1909 to 843 arcsec. Moreover, a-plane GaN with 3D buffer thicknesses larger than 600 nm had triangular pits on the surface. The optimized 3D GaN buffer thickness in this growth scheme was found to be around 600 nm. Nomarski optical microscope images of a-plane GaN with different 3D buffer thicknesses are shown in Fig. 3. 3. Fig 5. 3(a) and (b) show pitted and pit-free surfaces on the a-plane GaN grown with 3D buffer thicknesses of 1.2 μm and 600 nm, respectively. An atomic force microscope (AFM) image of the a-plane GaN is shown in Fig. 3. 4, with a root-mean-square roughness value of 0.43 nm when measured over a 4 x 4 μm^2 area, clearly indicating that a-plane GaN has triangular pit-free and atomically flat surface.

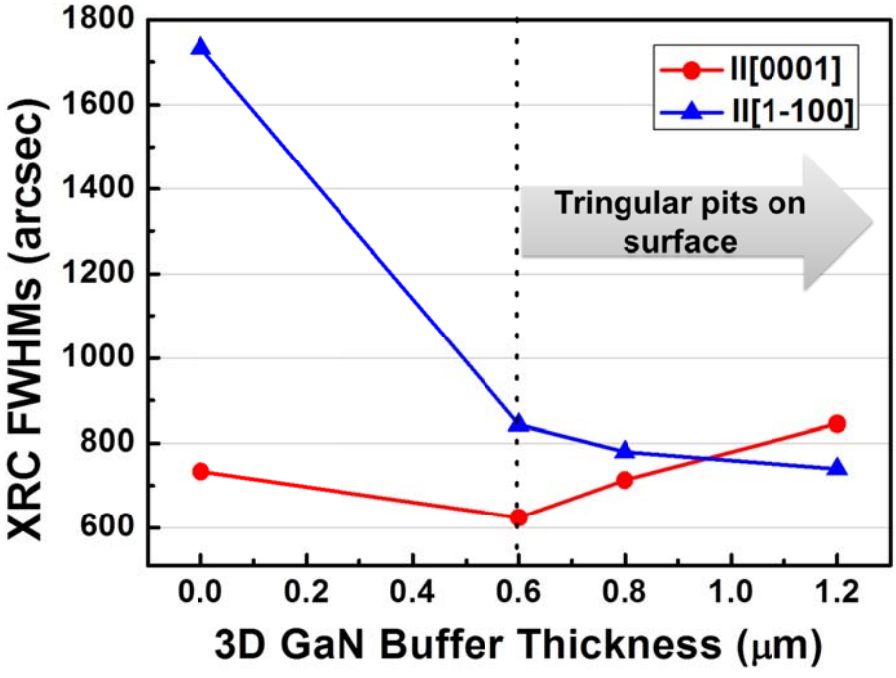

Fig. 3. 2 XRC FWHM of a-plane GaN at various thicknesses of the 3D GaN buffer layer

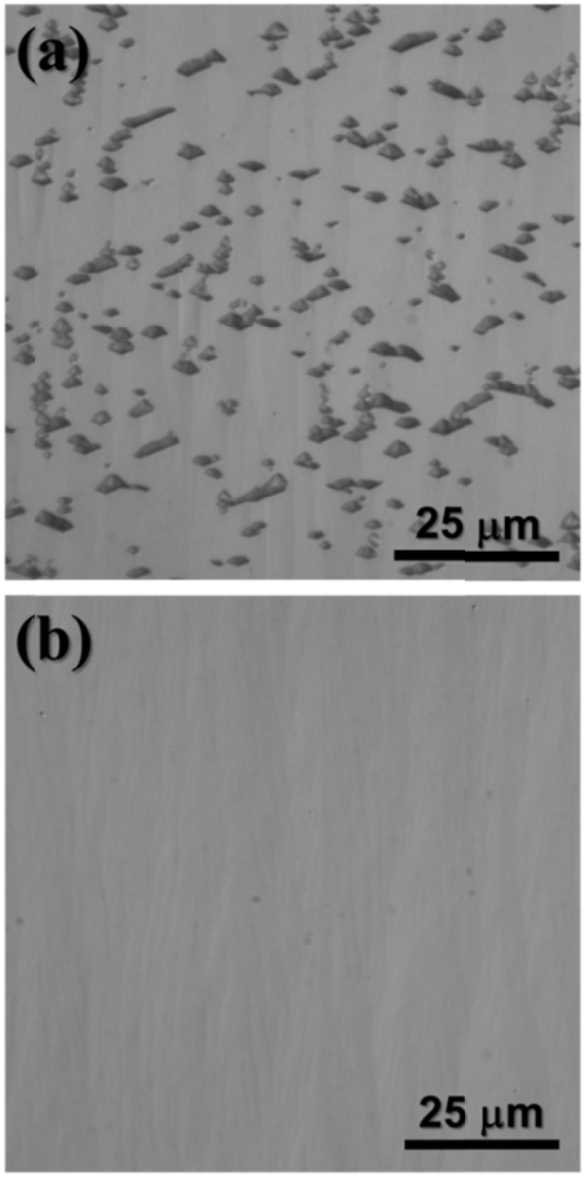

Fig. 3. 3 Nomarski optical microscope images of a-plane GaN with a 3D buffer layer for thicknesses of (a) 1.2 μm and (b) 600 nm.

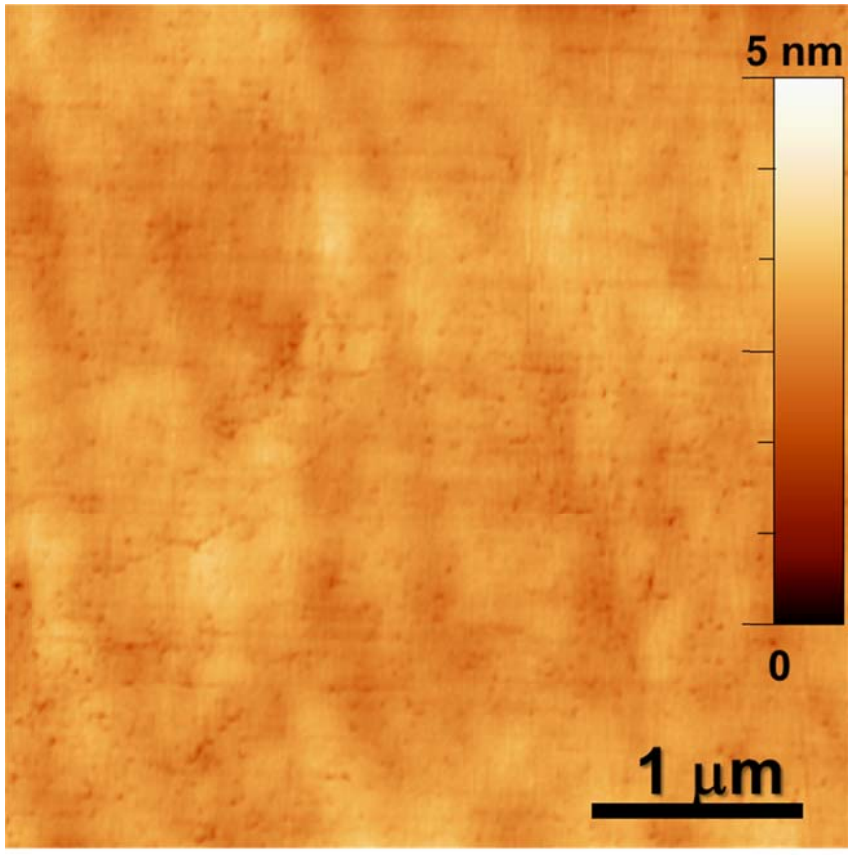

Fig. 3. 4 AFM images of a-plane GaN grown with the optimized 3D GaN buffer layer of 600 nm.

3.4. Fabrication of a-GaN LED with 3D shaped a-plane GaN buffer layer

To evaluate the device application for the a-plane GaN with a 3D GaN buffer layer, we fabricated nonpolar InGaN/GaN LEDs on the a-plane GaN template. The lateral-type LED structures consist of n-type GaN, three pairs of InGaN/GaN multiple quantum well layers, and p-type GaN. Indium-tin oxide (ITO) and Ti/Al/Ti/Au were used as the p- and the n-type contact materials, respectively. The LED shows a blue emission of 479.2 nm at an injection current of 20 mA.

First, we investigated the current-voltage (I-V) characteristic of the a-plane GaN LED with size of 350 x 350 μm^2. The current-voltage curve shows a rectifying behavior with a forward voltage (V_f) of 4.25 V at 20 mA, as shown in Fig. 3. 5(a). Reported forward voltage values varied from 4.61 V [12] to 3.36 V [13]. Further improvements in the LED fabrication process, such as contact annealing and improved crystal quality of a-plane GaN by better MOCVD growth, may lower the forward voltage at 20 mA. Changes in the electroluminescence (EL) emission wavelength of the a-plane GaN LED with injection current (on-wafer test) are shown in Fig. 3.5(b). The emission peak wavelength was shifted from 480.2 nm at 10 mA to 482.9 nm at 140 mA. The negligible wavelength shift of 2.7 nm with increasing drive

current is consistent with the minimal polarization-related internal electric fields in nonpolar a-plane GaN LEDs.

The variation of the EL characteristics with respect to injection currents ranging from 10 mA to 140 mA was assessed. The EL FWHMs and peak wavelength are summarized in Fig. 3. 6. A blue shift in the emission wavelength was observed in the low-current range less than 40 mA, suggesting that localized states formed by potential fluctuations were gradually occupied by injected carriers and that higher energy levels with higher density of states began to contribute to the EL emission [14]. For the broadening of the EL FWHM in the higher current range larger than 40 mA, we find that the broadening is accompanied by redshift of the EL peak in the LED [13], most probably due to the heat generation caused by the continuous-wave on-wafer probing.

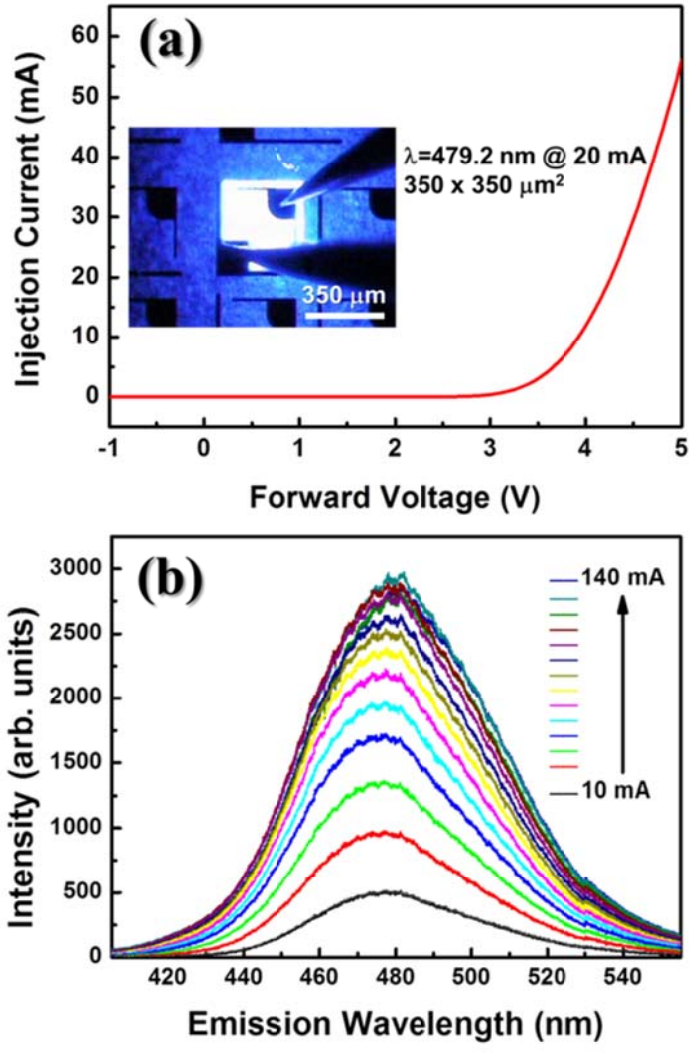

Fig. 3. 5 (a) Current-voltage characteristic of a-plane GaN LED with a 3D GaN buffer layer. The inset shows the blue emission of the a-plane GaN LED at an injection current of 20 mA. (b) EL spectra of the a-plane GaN LED.

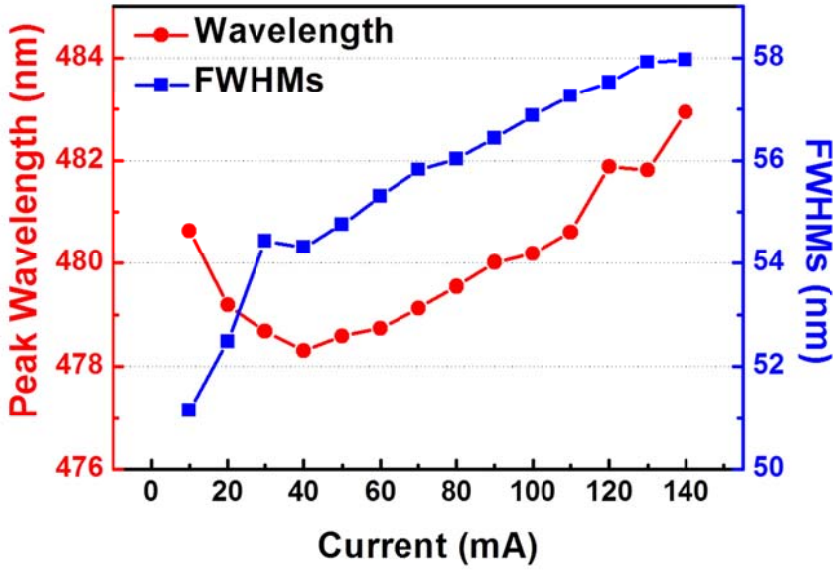

Fig. 3. 6 EL peak wavelength and FWHMs for injection currents ranging from 10 mA to 140 mA.

3.5. Conclusion

In conclusion, the effect of a 3D GaN buffer layer on the morphological and the crystalline properties of a-plane GaN grown by using MOCVD was investigated. The insertion of a 3D buffer layer is an effective method to obtain pit-free a-plane GaN with improved crystalline quality on r-plane sapphire substrates. Furthermore, an a-plane GaN LED with a 3D a-plane GaN buffer layer was characterized. The small wavelength shift with increasing drive current is consistent with the minimal polarization-related internal electric fields in nonpolar a-plane GaN LEDs.

3.6. References

[1] M. D. Craven, S. H. Lim, F. Wu, J. S. Speck, and S. P. DenBaars, Appl. Phys. Lett. 81, 469 (2002).

[2] Q. Sun, C. D. Yerino, T. S. Ko, Y. S. Cho, I.-H. Lee, J. Han and M. E. Coltrin, J. Appl. Phys. 104, 093523 (2008).

[3] F. Wu, M. D. Craven, S. H. Lim, and J. S. Speck, J. Appl. Phys. 94, 942 (2003).

[4] X. Ni, Y. Fu, Y. T. Moon, N. Biyikli, and H. Morkoç, J. Cryst. Growth 290, 166 (2006).

[5] S-N. Lee, H. S. Paek, J. K. Son, T. Sakong, O. H. Nam, and Y. Park , J. Cryst. Growth 307, 358 (2007)

[6] M. Araki, K. Hoshino, and K. Tadatomo, Jpn. J. Appl. Phys. 47, 119 (2008).

[7] S. H. Park, J. Park, D. Moon, N. Kim, D-J. You, J. Kim, J. Kang, S-M. Lee, J-S. Kim, M-S. Yang, T. Kim, and E. Yoon, J. Korean Phys. Soc. 58, 906 (2011).

[8] Z. H. Wu, A. M. Fischer, F. A. Ponce, T. Yokogawa, S. Yoshida, and R. Kato, Appl. Phys. Lett. 93, 011901 (2008).

[9] T. S. Ko, T. C. Wang, R. C. Gao, H. G. Chen, G. S. Huang, T. C. Lu, H. C. Kuo, and S. C. Wang, J. Cryst. Growth 300, 308 (2007).

[10] S. M. Hwang, Y. G. Seo, K. H. Baik, I-S. Cho, J. H. Baek, S. Jung, T. G. Kim, and M. Cho, Appl. Phys. Lett. 95, 071101 (2009).

[11] T. Sasaki , J. Cryst. Growth 129, 81 (1993).

[12] D. H. Kim, S. J. Kim, S. H. Kim, T. Jeong, S. M. Hwang, and T. G. Kim, Phys. Status Solidi RRL 5, 274 (2011).

[13] K. H. Baik, J-H. Park, S-H. Lee, H. Song, S-H. Hwang, S. Lee, J. Jhin, J. Tak, and J. Kim, J. Korean Phys. Soc. 56, 1140 (2010).

[14] M. Funato, M. Ueda, Y. Kawakami, Y. Narukawa, T. Kosugi, M. Takahashi and T. Mukai, Jpn. J. Appl. Phys. 45, 26, L659 (2006).

Chapter 4. Growth of nonpolar a-plane GaN with silica nano-spheres

4.1. Introduction

Wurtzite GaN-based light emitting diode (LED) structures grown along the c-axis suffer from strong polarization related to internal electric fields, which induce the spatial separation of electrons and holes in the active layers and a resulting red-shift of the emission wavelength due to the quantum confined Stark effect [1]. To prevent these adverse effects, several groups have tried to grow GaN-based LED structures on nonpolar planes, such as the a-plane or m-plane [2,3]. To achieve high efficiency nonpolar LEDs for general illumination, the development of high quality nonpolar GaN epitaxial layers with a low defect density and a cost-effective technique to improve the light extraction efficiency of LEDs are required.

Although nonpolar GaN substrates with high crystallinity can be obtained by slicing a thick c-plane GaN wafer grown by hydride vapor phase epitaxy (HVPE),[4] $(1\bar{1}02)$ r-plane sapphire is still the most commonly used large-area substrate for a-plane GaN growth, due to its relatively low cost.

However, the major drawback of r-plane sapphire substrates for the

growth of nonpolar a-plane GaN is the high defect density in the a-plane GaN epitaxial layer. These defects mainly originate from the 16 % difference in the lattice constants between a-plane GaN and r-plane sapphire along the m-direction of GaN, resulting in high density, non-radiative recombination centers in a-plane GaN LEDs [3]. In addition, the enhanced in-plane growth rate anisotropy of a-plane GaN on r-plane sapphire results in the 3-dimensional (3D) growth of a-plane GaN. This 3D growth leaves a large number of micrometer-scale triangular pits on the GaN surface during the coalescence of the islands [3,5,6].

To prevent the formation of rough surfaces and/or triangular pits in a-plane GaN, most research groups have tried to grow nonpolar GaN at relatively low pressures to enhance the formation of islands in the nucleation layer [5-8]. This growth condition facilitated the coalescence of a-plane GaN at the early stage of growth, leading to pit-free surfaces. However, the coalesced surface formed at low pressure is usually grown at the expense of numerous threading dislocations in the epitaxial layer, due to the increased number of islands formed during its growth. To improve the crystalline quality of a-plane GaN, several research groups have reported the use of conventional epitaxial lateral overgrowth (ELO) or a modified ELO process on top of low-pressure-grown a-plane GaN with high threading dislocation

density.[9-11] However, such ELO processes resulted in long processing times and, hence, high cost, due to the complexity of such processes as mask deposition and etching.

To overcome these obstacles, we utilized the 3D growth nature of a-plane GaN and controlled integration of silica nano-spheres into the rough GaN buffer layer to improve the crystalline quality of nonpolar a-plane GaN. In addition to the crystalline quality improvement by silica nano-spheres, the silica nano-spheres integrated in the GaN can improve the light extraction efficiency (LEE) of GaN-based LEDs. Nanometer-scale silica spheres act as internal scattering centers of the light emitted from the active layer of the LEDs. Thus, the angle of reflected light at the GaN/sapphire interface is distributed over a wide range of angles. Therefore, the LEE of GaN-based LEDs is increased by the enhanced probability of entering escape cone defined by the critical angle for total internal reflection [15].

4.2. Experimental procedure

r-plane sapphire wafers (-0.2 ± 0.05^{o} off toward the m-axis of sapphire) were used as the substrates. The entire growth process for the CIS a-plane GaN was performed using a Thomas Swan 3 x 2 inch MOCVD reactor with hydrogen as a carrier gas and trimethylgallium and ammonia as precursors in the GaN growth process. The 3D-shaped a-plane GaN buffer layer was grown at a pressure of 300 torr. The controlled integration of the silica nano-spheres on the 3D a-plane GaN layer was performed using a spin coating method. The silica nano-spheres used in this experiment were dispersed in ethanol solution and their average diameter was 250 nm. For the overgrowth step on the silica nano-spheres, the growth pressure was decreased to 100 torr to promote the lateral growth of GaN. For the growth process, the V/III ratio and growth temperature were maintained at 380 and 1040 ^{o}C, respectively. The sample was characterized by SEM, CL, cross-sectional TEM, XRD, spectrophotometry and EL spectroscopy.

4.3. Growth of a-plane GaN by controlled integration of silica nano-spheres (CIS)

On r-plane sapphire, we intentionally fabricated a rough a-plane GaN buffer layer by metal-organic chemical vapor deposition (MOCVD) and selectively masked trench areas with silica nano-spheres. The silica nano-spheres blocked the propagation of the threading dislocations originating at the interface between the GaN and the sapphire substrate, and prevented the formation of additional islands on the substrate during the subsequent coalescence process at low pressure. In the case of the growth of polar c-plane GaN, techniques using silica spheres as an epitaxial lateral overgrowth (ELO) mask have been reported involving the use of coated silica micro-spheres on the flat GaN surface or silica nano-spheres embedded in the wet-etched GaN surface [12-14]. In this study, neither complex chemical etching nor a uniform distribution of silica spheres on the flat surface of GaN was necessary, since the as-grown textured 3D nonpolar GaN surface can be readily used for the preferential coating of silica nano-spheres in the recessed areas formed by nonpolar GaN growth.

For the selective masking of the trench areas of the 3D-shaped a-plane GaN by the silica nano-spheres, a spin coating method was used, based on recent studies in which the trenches were filled with nanoparticles [16-18].

Using the controlled integration of silica nano-spheres (CIS) into the 3D-shaped nonpolar GaN buffer layer and the subsequent ELO, we demonstrated a more effective, simplified and controllable epitaxial layer growth process which improves the crystal quality of nonpolar GaN and the extraction efficiency of the LEDs without the need for any intentional surface roughening to improve the light extraction or the complicated SiO_2 or SiN_X mask deposition and patterning processes employed in the conventional ELO processes [9-11]. A schematic of the CIS and regrowth process is illustrated in Fig. 4. 1.

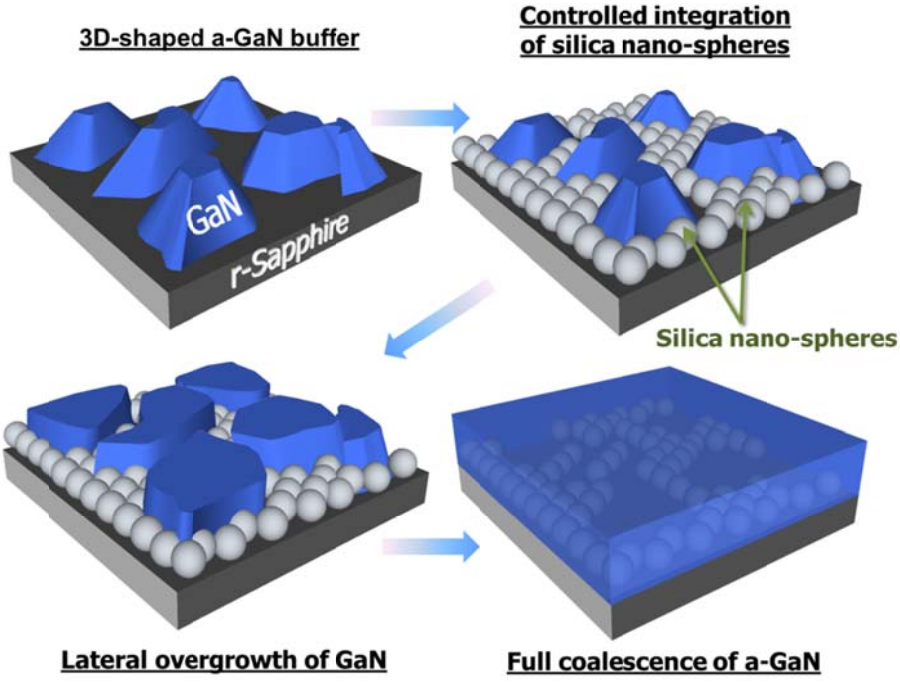

Fig. 4. 1 Scheme of the CIS growth process: 3D-shaped a-plane GaN buffer; controlled integration of silica nano-spheres on 3D-shaped a-plane GaN buffer; lateral growth of GaN on the integrated silica nano-spheres; full coalescence of the CIS a-plane GaN.

A 3D-shaped a-plane GaN buffer layer (1-μm-thick) with various facets such as $\{1\bar{1}01\}$ and $(000\bar{1})$ was grown, as shown in Fig. 4. 2. Then, silica nano-spheres with a diameter of 250 nm were preferentially integrated in the trench area of the 3D buffer layers by using a conventional spin coating method. The silica nano-spheres from an aqueous colloidal suspension were spread out on the substrate and integrated into the trench areas of the 3D GaN layer by evaporating the solution and subsequently displacing the silica nano-spheres to the trench area during the spin coating process [16-18] as shown in Fig. 4. 3. Fig. 4. 4 shows a scanning electron microscopy (SEM) image of the a-plane GaN buffer layer with silica nano-spheres integrated in the trench area. During the GaN regrowth on this CIS GaN buffer layer at high temperature, the silica nano-spheres, which are preferentially integrated into the trenches of the 3D shaped a-plane GaN buffer layer, act as a mask for the subsequent ELO process.

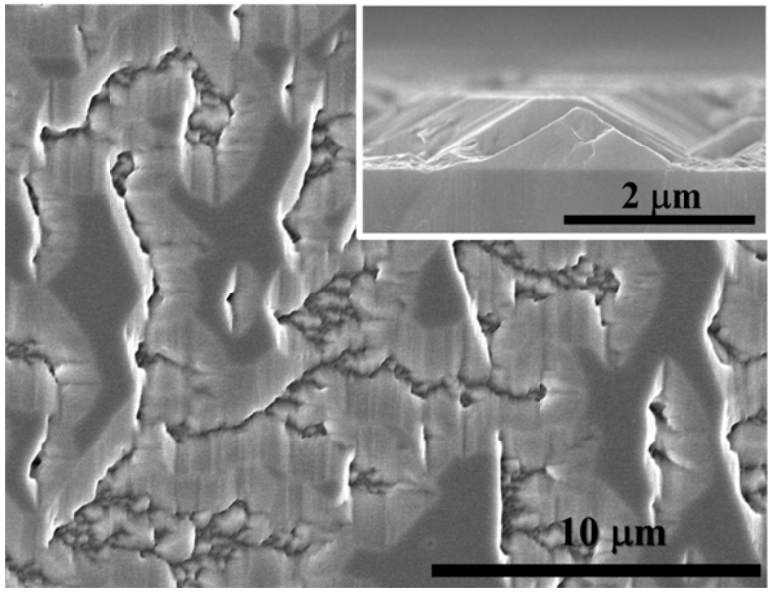

Fig. 4. 2 (a) SEM image of 3D-shaped a-plane GaN buffer. Inset: cross-section SEM image of GaN buffer.

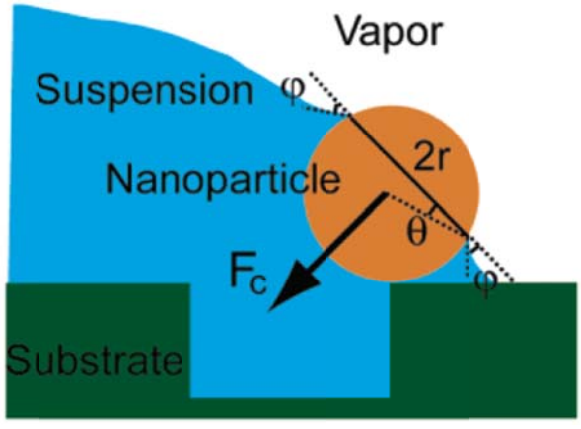

Fig. 4. 3 Integration of nano-spheres into trench on the surface; Evaporation of the solvent → Capillary force slides the nano-sphere toward the thick part of the solution→ Particles are selectively forced into the trenched feature [17].

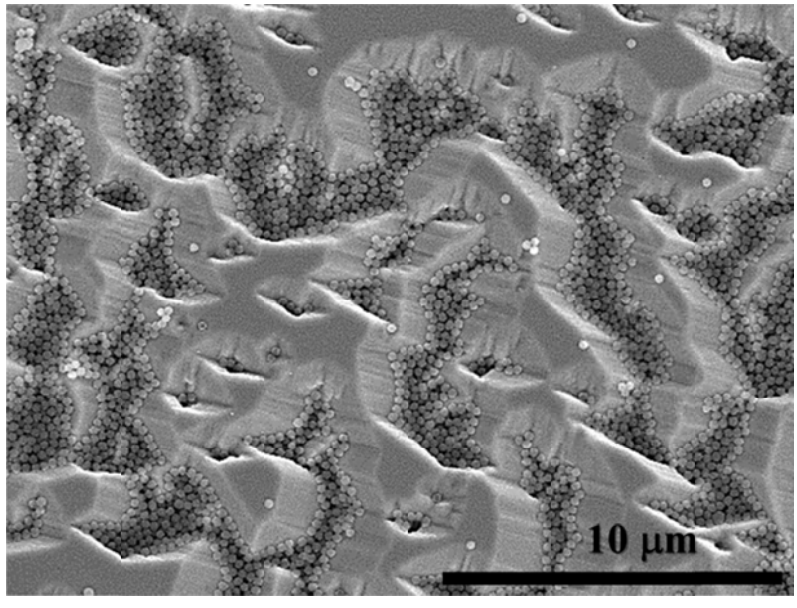

Fig. 4. 4 SEM image of controlled integration of silica nano-spheres on 3D-shaped a-plane GaN buffer by spin coating method.

In the Nomarski optical microscope image of the a-plane GaN surface grown by the CIS and regrowth process, a fully coalesced surface is observed with slight contrast differences, implying that the trench area, in which the silica nano-spheres are integrated, can be observed by an optical microscope, as shown in Fig. 4. 5(c). Fig. 4. 5(d) shows a cross-section SEM image of the a-plane GaN after the CIS and regrowth process. The laterally grown a-plane GaN epitaxial layers on the integrated silica nano-spheres are fully coalesced without the triangular pits commonly observed in the surface of the a-plane GaN.

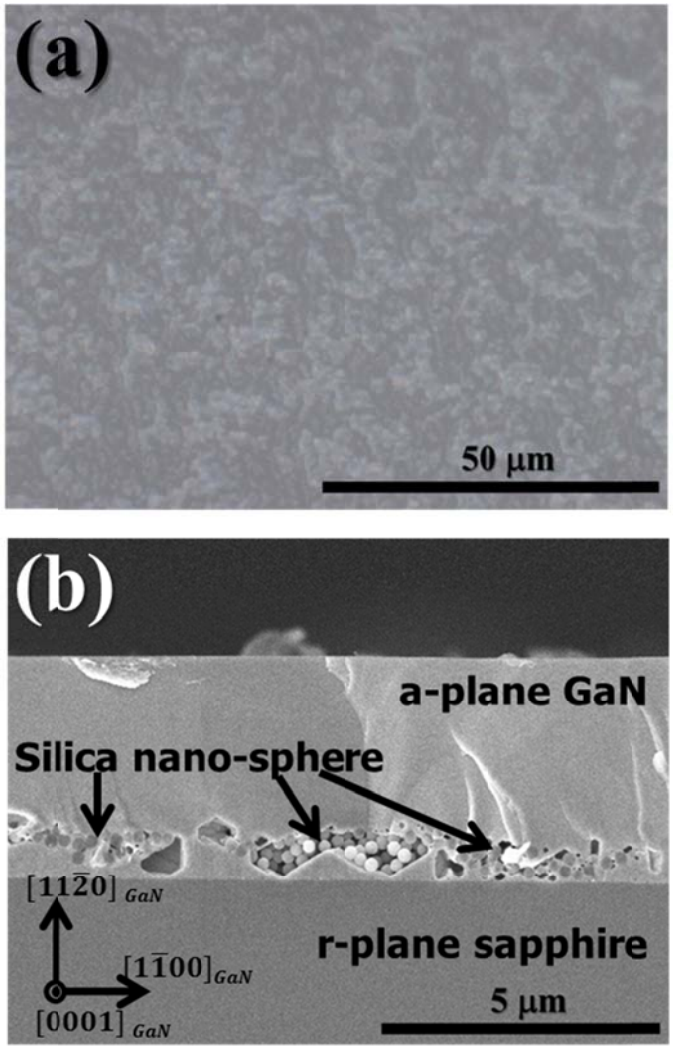

Fig. 4. 5 (a) Nomarski optical microscope image of fully coalesced CIS a-plane GaN surface. (b) Cross-section SEM image of full coalescence of the CIS a-plane GaN

4.4. Reduced defects density of CIS a-plane GaN

Cathodoluminescence (CL) measurements were used to investigate the luminescence properties relating to the nonradiative recombination in the CIS a-plane GaN epitaxial layer. A plan-view CL image obtained at 77 K in order to compare the CIS a-plane GaN to the a-plane GaN without CIS is shown in Figs. 4. 6(a) and (b). Due to the low defect density of the GaN layer overgrown on the CIS a-plane GaN in Fig. 4. 6(a), the bright contrast surface was increased by 74 % compared to the surface of the a-plane GaN without CIS in Fig. 4. 6(b). Fig. 4. 7(a) is the cross-sectional CL image of the CIS a-plane GaN layer viewed along the [0001] direction of GaN. The region formed by ELO above the integrated silica nano-spheres appears brighter. The cross-sectional transmission electron microscopy (TEM) image viewed along the GaN $[1\bar{1}00]$ direction shows the dislocation distribution in the CIS a-plane GaN epitaxial layer in Fig. 4. 7(b). From the CL and TEM analysis, we confirmed that the threading dislocations originating from the interface between the GaN and sapphire substrate were blocked by the integrated silica nano-spheres. Therefore, the laterally overgrown a-plane GaN layers on the silica nano-spheres had a reduced dislocation density along with improved crystalline quality and optical properties.

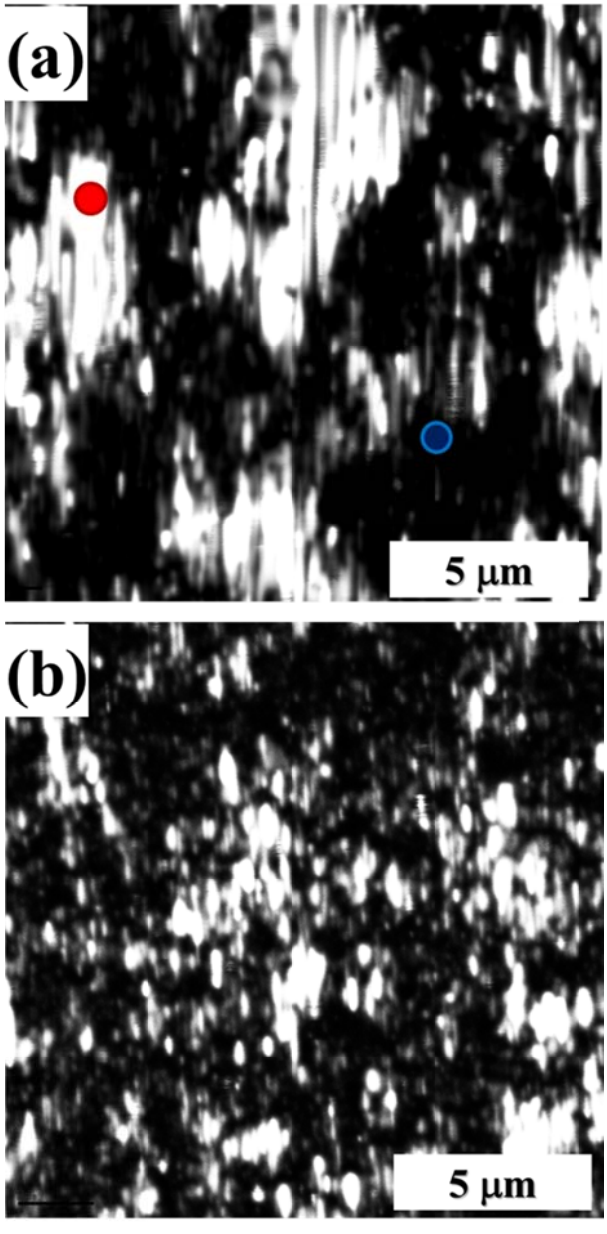

Fig. 4. 6 Plan-view CL images of (a) CIS a-plane GaN and (b) reference a-plane GaN measured at 77 K. The red and blue circle in (a) represent the excitation point from the spot beam shown in Fig. 4. 8.

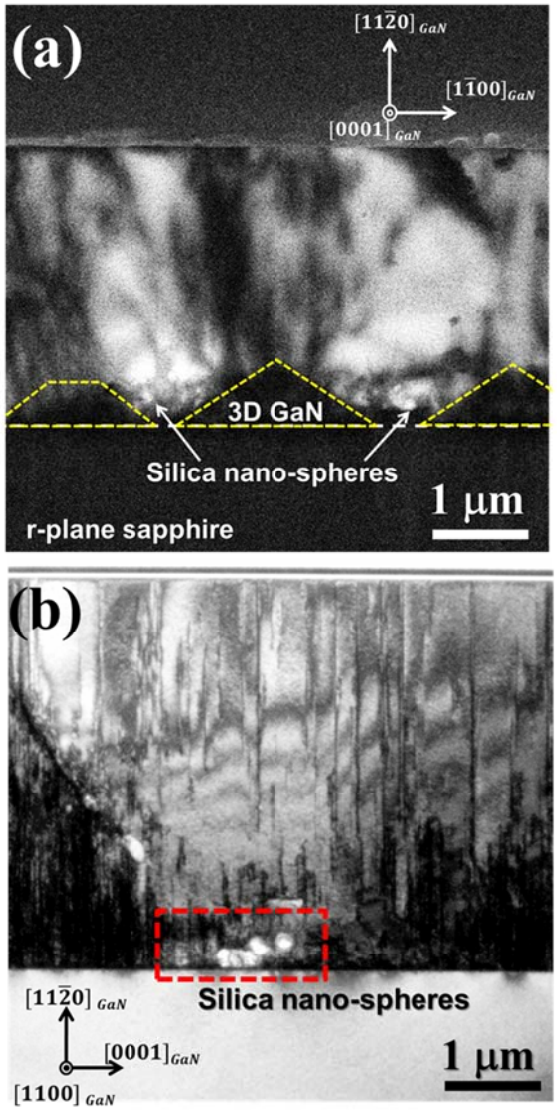

Fig. 4. 7 (a) Cross-sectional CL image of CIS a-plane GaN view along the [0001] direction of GaN. (b) Cross-section TEM bright field image of CIS a-plane GaN viewed along the direction of GaN showing the dislocation blocking by the integrated silica spheres. The dashed box (in red) shows the integrated silica spheres.

The CL spectra measured from the red and blue spots marked in Fig. 4. 6(a) demonstrate that the emission mainly came from the basal plane stacking faults (BSFs) with an emission energy of 3.44 eV, as shown in Fig. 4. 8. The BSF emission is attributed to the ultrathin quantum well (QW) layer formed by the insertion of zinc-blende phase GaN in the surrounding wurtzite, which corresponds to I1-type BSFs [19]. From the emission spectrum of blue spot in the dark region, the reduced BSF emission intensity is due to the nonradiative recombination caused by the dislocations in the region where both dislocations and BSFs are present in large number. The emission at 3.36 eV presumably comes from the prismatic plane stacking faults (PSFs) which existed at the end of the BSFs of the a-plane GaN [20, 21]. Our spectra also show phonon replicas at several low-energy sidebands separated from the peak at 3.31 eV by ~90 meV, indicating moderate coupling with the LO phonons [19]. The feature at 3.31 eV is attributed to a donor-acceptor pair (DAP) emission, which seems to be related to the PSFs and impurity incorporation near the PSFs.

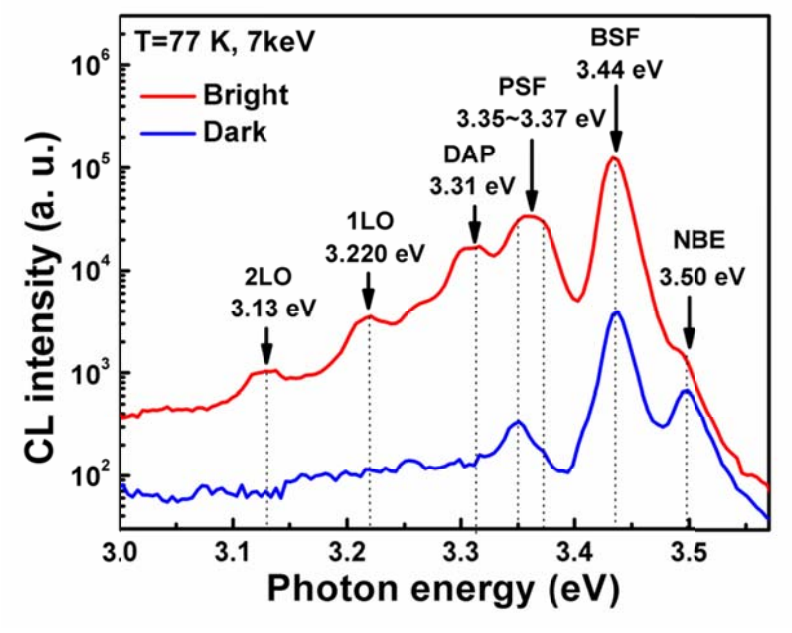

Fig. 4. 8 CL spectra of CIS a-plane GaN measured from the spot beam excitation. The red and blue circle in Fig. 6. 6(a) represent the excitation point from the spot beam.

High resolution X-ray diffraction (XRD) was used to study the crystalline quality of the CIS a-plane GaN over a large sample area. As shown in Fig. 4. 9, the full width at half maximum (FWHM) in the XRD rocking curve of the CIS a-plane GaN was decreased to 580 and 550 arcsec along the c-direction and m-direction of GaN, as compared to 632 and 843 arcsec for the a-plane GaN grown without silica nano-spheres, respectively. This result is consistent with the low defect density and extended emission area on the surface of the a-plane GaN layer, confirming the significant improvement in the crystalline quality of the CIS GaN as compared with the a-plane GaN grown without silica spheres. Although the crystalline quality of the CIS a-plane GaN was not as high as the best values previously reported for a-plane GaN [11, 22], it could be further improved by optimizing the coverage of the integrated silica nano-spheres and subsequent ELO process.

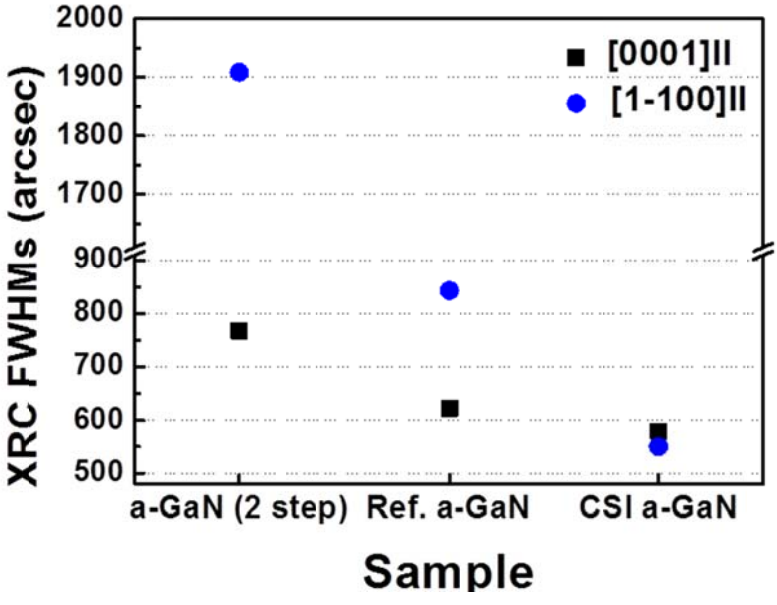

Fig. 4. 9 X-ray rocking curve full width at half maximums of reference a-plane GaN and CIS a-plane GaN

To verify the substantial reduction in the densities of both BSFs and dislocation, we carried out plan-view TEM study on reference a-plane GaN and CIS a-plane GaN. Most of the observed BSFs were I_1 type, normally bounded by Frank-Shockley partial dislocations (PDs) (**b**=1/6<2-203>). There were some I_2 type BSFs bounded by Shockley PDs (**b**=1/3<1-100>), as well as a few PSFs interconnecting adjacent BSFs. The dislocations observed in the plan-view were all partials according to the one-to-one location correlation between the ends of the BSFs and PDs. No perfect dislocations were observed in the view although the diffraction configurations adopted in this study did satisfy the visibility criteria for perfect dislocations [23]. By definition, perfect dislocation has a BV of a completed translation vector of the lattice, such as [0001]. In contrast, the BV of a PD is not a complete translation vector of the lattice, such as 1/2[0001]. As revealed in Fig. 4. 10, the PD density of CIS a-plane GaN (~5.6 X 10^9 cm^{-2}, average value of less defective area above silica nano-spheres ~ 1 X 10^9 cm^{-2} and defective area without silica nano-sphere ~ 1.1 X 10^{10} cm^{-2}) was lower than that of reference a-plane GaN (~1.1 X 10^{10} cm^{-2}), which was consistent with the difference in the XRC FWHMs between the two samples.

By calculating the total length of the observed BSFs divided by the image

area, we estimated the BSF density in the a-plane GaN to be ~ 3.4 X 10^5 cm^{-1} and 2.7 X 10^5 cm^{-1} for sample without and with silica nano-spheres, respectively. We need further investigation to find out the reason for negligible decrease of BSF density in CIS a-plane GaN.

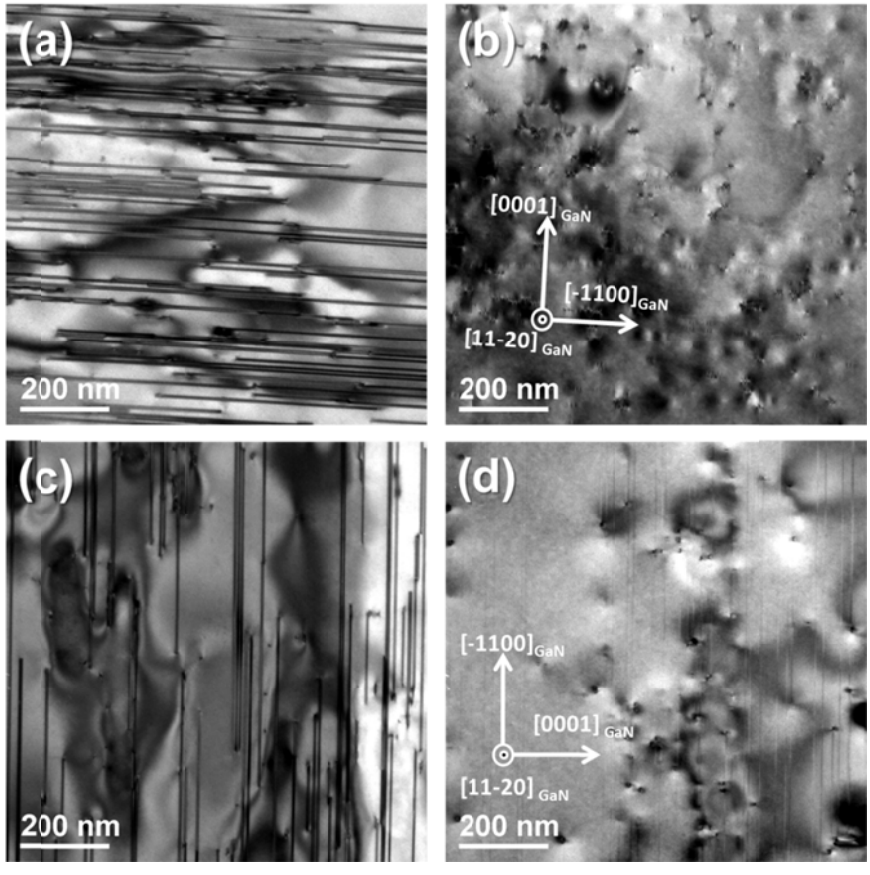

Fig. 4. 10 Plan-view TEM images of reference a-plane GaN [(a) and (b)] and CIS a-plane GaN [(c) and (d)]. The **g** vectors were 1-100 for (a) and (c), and 0002 for (b) and (d), to reveal the SFs and PDs, respectively.

4.5. Reflectance enhancement of CIS a-plane GaN

To confirm the effect of the silica nano-spheres on the light extraction of GaN, we investigated the diffuse reflectance of the CIS a-plane GaN epitaxial layers by collecting the light scattered at all angles by using an integrating sphere. The incident light has an angle of 8 degree from surface normal. The schematic of diffuse reflectance was shown in Fig 4. 11.

Fig. 4. 12 shows that the total reflectance of the CIS a-plane GaN is higher than that of the conventional a-plane GaN without the CIS process. The Fresnel reflection caused from the interface of air (n=1) and GaN (n=2.43) have value of 17.7 % when incident light (wavelength =480 nm) has the angle of 8 degree from the surface normal. The total reflection of CIS a-plane GaN was enhanced by about 30 ~ 38 % in the wavelength range from 400 to 700 nm when we compared to the value of reference a-plane GaN. From the simple extraction the Fresnel reflection from the total reflectance, we can observed that about 10 % for reference a-plane GaN and 20 % for CIS a-plane GaN of reflection enhancement were originated from the GaN and sapphire (n=1.7) interface. Since the surface root-mean-square (RMS) roughness of the samples measured by atomic force microscopy (AFM) over a 4 x 4 μm^2 area was almost constant with a value of 0.5 ± 0.1 nm, this enhancement is attributed to the increased probability of the

escaping photons undergoing diffuse reflection and scattering by the silica nano-spheres in the GaN layer.

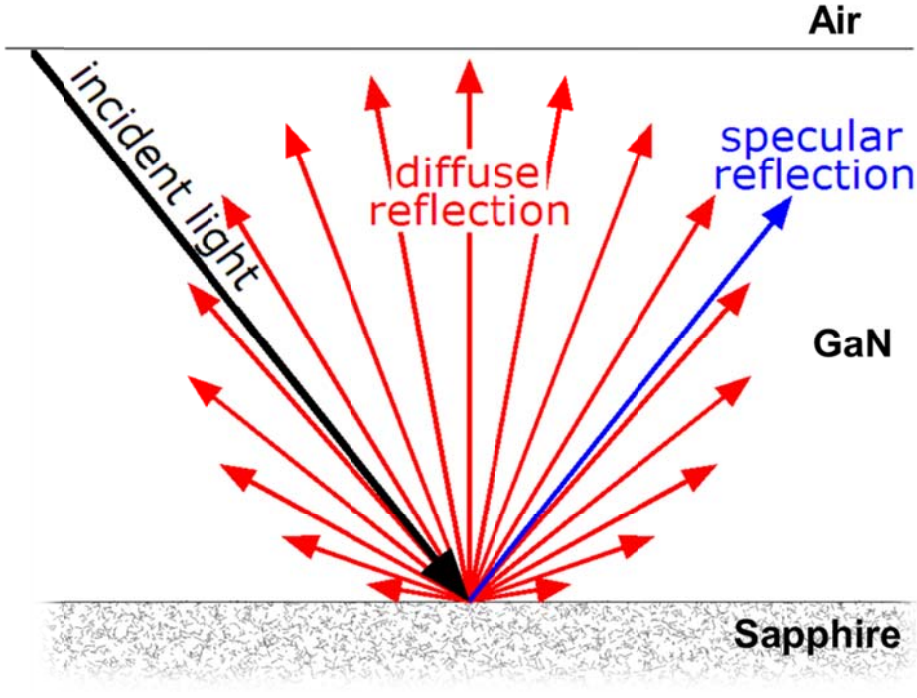

Fig. 4. 11 Diffuse and specular reflection from a sapphire substrate surface. [Image from commons.wikimedia.org]

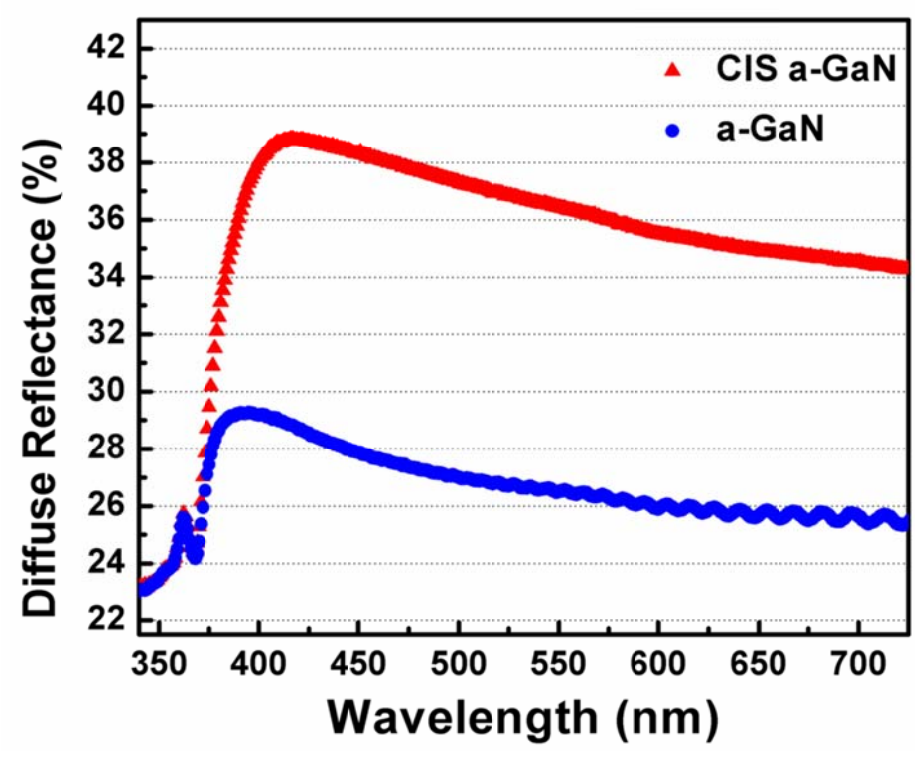

Fig. 4. 12 Diffuse reflectance spectra of CIS a-plane GaN and reference a-plane GaN without CIS process.

4.6. Conclusion

In conclusion, a novel, simple and inexpensive efficiency improvement technique of crystalline quality employing silica nano-spheres is proposed. The 3-dimensional growth nature of a-plane GaN was utilized to from the regrowth template of a-plane GaN. Subsequently, the controlled integration of silica nano-spheres (CIS) into the regrowth template is performed to improve the crystal quality of a-plane GaN by epitaxial lateral overgrowth (ELO) method. The silica nano-spheres were used as the mask layer for the regrowth of nonpolar a-plane GaN with reduced threading dislocation density during subsequent ELO process. In addition, the CIS improves light reflection by the scattering process. This scattering process enhances the light extraction of a-plane GaN LEDs. We expect that the optimization of the CIS growth process on nonpolar GaN will lead to further improvements, such as the lowering of the extended defect density and improvement of the extraction efficiency of nonpolar LEDs.

4.7. References

[1] D. A. B. Miller, D. S. Chemla, T. C. Damen, A. C. Gossard, W. Wiegmann, T. H. Wood and C. A. Burrus, Phys. Rev. Lett. 1984, 53, 2173.

[2] P. Waltereit, O. Brandt, A. Trampert, H. T. Grahn, J. Menniger, M. Ramsteiner, M. Reiche and K. H. Ploog, Nature 2000, 406, 865.

[3] M. D. Craven, S. H. Lim, F. Wu, J. S. Speck and S. P. DenBaars, Appl. Phys. Lett. 2002, 81, 469.

[4] K. C. Kim, M. C. Schmidt, H. Sato, F. Wu, N. Fellows, Z. Jia, M. Saito, S. Nakamura, S. P. DenBaars and J. S. Speck, Appl. Phys. Lett. 2007, 91, 181120.

[5] X. Ni, Y. Fu, Y. T. Moon, N. Biyikli, and H. Morkoç, J. Cryst. Growth 2006, 290, 166.

[6] Q. Sun, C. D. Yerino, T. S. Ko, Y. S. Cho, I.-H. Lee, J. Han and M. E. Coltrin, J. Appl. Phys. 2008, 104, 093523.

[7] T. S. Ko, T. C. Wang, R. C. Gao, H. G Chen, G. S. Huang, T.C. Lu, H. C. Kuo, J. Cryst. Growth 2007, 300, 308.

[8] S.-N Lee, H. S. Paek, J. K. Son, T. Sakong, O. H. Nam, Y. Park , J. Cryst. Growth 2007 307, 358.

[9] F. Wu, M. D. Craven, S. H. Lim, and J. S. Speck, J. Appl. Phys. 2003, 94, 942.

[10] Q. Li, Y. Lin, J. R. Creighton, J. J. Figiel and G. T. Wang, Adv. Mater. 2009, 21, 2416.

[11] D. Iida, M. Iwaya, S. Kamiyama, H. Amano and I. Akasaki, J. Cryst. Growth 2009, 311, 2887.

[12] S. J. An, Y. J. Hong, G. C. Yi, Y. J. Kim and D. K. Lee, Adv. Mater. 2006, 18, 2833.

[13] Q. Li, J. J. Figiel and G. T. Wang, Appl. Phys. Lett. 2009, 94, 231105.

[14] Y. J. Park, H. Y. Kim, J. H. Ryu, H. K. Kim, J. H. Kang, N. Han, M. Han, H. Jeong, M. S. Jeong and C.-H. Hong, Opt. Express 2011, 19, 2029.

[15] E. F. Schubert, in Light-Emitting Diodes, second edition, Cambridge University Press, Cambridge, United Kingdom 2006, Ch. 5.

[16] Y. Xia, Y. Yin, Y. Lu and J. McLellan, Adv. Funct. Mater. 2003, 13, 907.

[17] Y. Cui, M. T. Björk, J. A. Liddle, C. Sönnichsen, B. Boussert and A. P. Alivisatos, Nano Lett. 2004, 4, 1093.

[18] S. M. de Sousa Pereira, M. A. Martins, T. Trindade, I. M. Watson, D. Zhu and C. J. Humphreys, Adv. Mater. 2008, 20, 1038.

[19] P. P. Paskov, R. Schifano, B. Monemar, T. Paskova, S. Figge and D. Hommel, J. Appl. Phys. 2005, 98 093519.

[20] R. Liu, A. Bell, F. A. Ponce, C. Q. Chen, J. W. Yang and M. A. Khan, Appl. Phys. Lett. 2005, 86, 021908.

[21] J. Mei, S. Srinivasan, R. Liu, F. A. Ponce, Y. Narukawa and T. Mukai, Appl. Phys. Lett. 2006, 88, 141912.

[22] S.-M. Hwang, Y. G Seo, K. H.Baik, I.-S. Cho, J. H. Baek, S. Jung, T. G. Kim, M. Cho, Appl. Phys. Lett. 2009, 95, 071101.

[23] Q. Sun, B. h. Kong, C. D. Yerino, T.-S. Ko, B. Leung, H. K. Cho, and J. Han, J. Appl. Phys., 106, 123519 (2009)

Chapter 5. Fabrication of a-plane GaN light emitting diodes with silica nano-spheres

5.1. Introduction

In order to improve the emission efficiency of nonpolar a-plane GaN light emitting diodes (LEDs) by a simple process, we have reported that the controlled integration of silica nano-spheres (CIS) into the a-plane GaN epitaxial layer grown on r-plane sapphire by metal-organic chemical vapor deposition [1]. First, we intentionally grew the 3-dimensional (3D), rough a-plane GaN buffer layer by using the anisotropic growth nature of a-plane GaN on r-plane sapphire. Then, the silica nano-spheres with diameter of 250 nm were preferentially integrated in the valley of the buffer layers by using a spin coating method. In this CIS process, the silica nano-spheres integrated in the valley act as SiO_2 mask layers in the subsequent epitaxial lateral overgrowth (ELO) process. In addition to the ELO effect by the silica nano-spheres, the silica nano-spheres integrated in the GaN can improve the light extraction efficiency (LEE) of GaN-based LEDs. Nanometer-scale stacked silica spheres act as internal scattering centers of the light emitted from the active layer of the LEDs. This internal light scattering changes the path of

the emitted light to the top surface of LEDs. Therefore, the LEE of CIS GaN-based LEDs are increased by the enhanced probability of entering escape cone defined by the critical angle for total internal reflection.

To evaluate the use of the CIS a-plane GaN in devices, we fabricated nonpolar InGaN/GaN LEDs on the CIS a-plane GaN template. The reference LED sample was fabricated using the same growth and fabrication process, except for the CIS process during the epitaxial growth.

5.2. Experimental procedure

The LED structures consist of 7-um-thick a-plane GaN template, 1.5-um-thick n-type a-plane GaN, three pairs of InGaN/GaN quantum well layers with 3-nm-thick InGaN and 12-nm-thick GaN and 150 nm-thick p-type a-plane GaN. The 60 second annealing was performed at 880 ^{o}C for the p-type activation. ITO and Ti/Al/Ti/Au were used as the p- and n-type contact materials, respectively. The LEDs were characterized by electroluminescence (EL), polarized EL, current-voltage measurements, light output power measurement. Finite-difference time-domain (FDTD) simulations of Lumerical Solutions were used to calculate the extraction efficiency and polarization ratio of LED structures. The schematic of CIS a-plane GaN LED fabrication was shown in Fig. 5. 1.

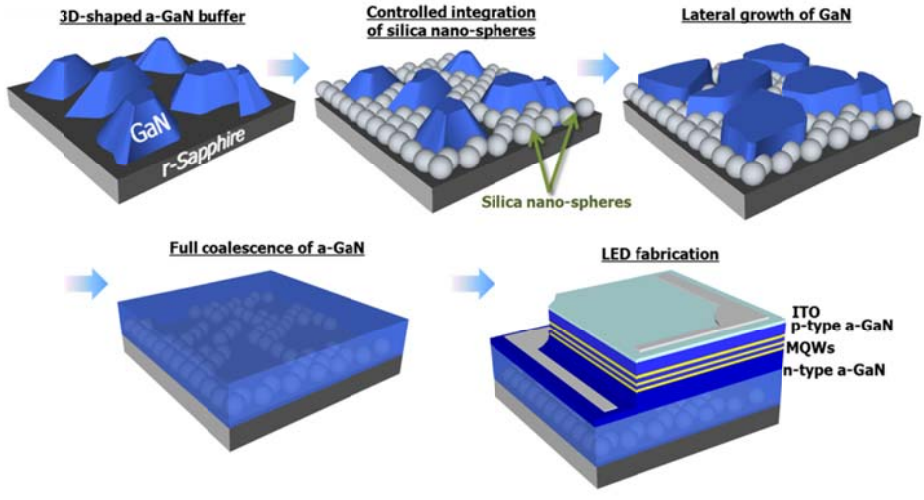

Fig. 5. 1 Scheme of the controlled integration of silica nano-spheres (CIS) and LED structures.

5.3. Optical properties of CIS a-plane GaN light emitting diode

Fig. 5. 2 shows the variation in the electroluminescence (EL) emission wavelength of the CIS a-plane GaN LED with the injection current (on-wafer test). The inset of Fig. 5. 2 shows the strong blue emission of the CIS a-plane GaN LED with 476.1 nm peak wavelength at an injection current of 20 mA. The emission peak wavelength was shifted from 477.3 nm at 10 mA to 476.5 nm at 100 mA. This negligible wavelength shift with increasing drive current is consistent with the minimal polarization-related internal electric fields in nonpolar a-plane GaN LEDs. The variation of the EL peak wavelength with respect to injection currents ranging from 10 mA to 100 mA was assessed. The EL peak wavelength is summarized in Fig. 5. 3. A blue shift in the emission wavelength was observed in the low-current range less than 40 mA, suggesting that localized states formed by potential fluctuations were gradually occupied by injected carriers and that higher energy levels with higher density of states began to contribute to the EL emission [2].

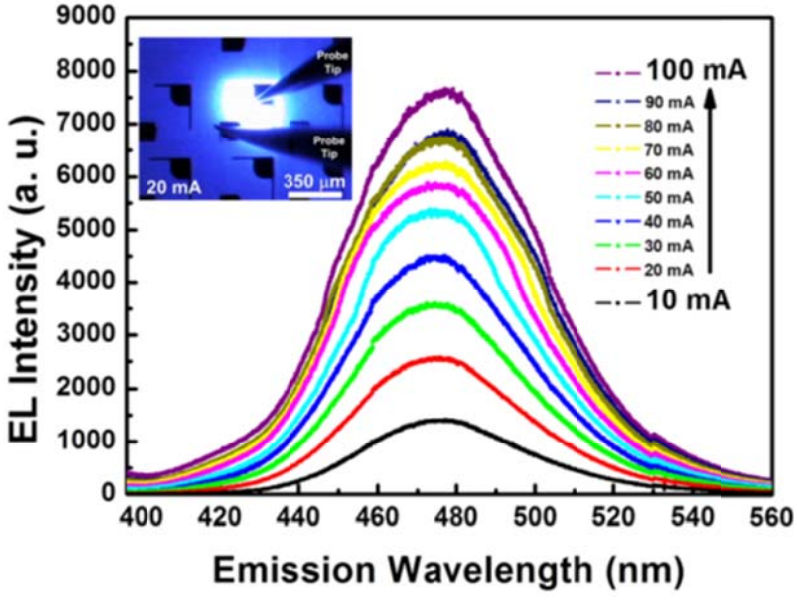

Fig. 5. 2 EL spectra of the CIS a-plane GaN LED with injection currents in the range from 10 mA to 100 mA. The inset shows the blue emission of the CIS a-plane GaN LED with 476.1 nm peak wavelength at an injection current of 20 mA.

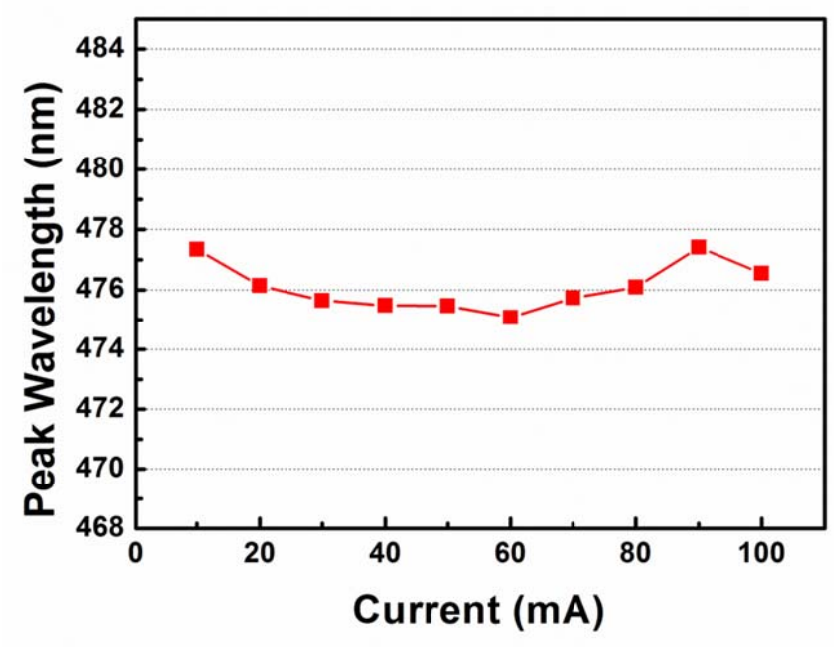

Fig. 5. 3 Electroluminescence peak wavelength of CIS a-plane GaN LED with injection current range from 2 mA to 100 mA

5.4. Polarization properties of CIS a-plane GaN LED

The interest in nonpolar orientations of the wurtzite crystal structure originates from the absence of internal electric fields in group-III-nitride-based heterostructures, which are expected to improve the efficiency of light emitting diodes. GaN films grown along the polar direction (C plane), which are usually unstrained or isotropically strained; do not exhibit any in-plane polarization anisotropy. In contrast, unstrained m- and a-plane GaN films, where the c axis lies in the film plane (cf. Figure 5. 4(a)), exhibit a significant in-plane polarization anisotropy with a degree of linear polarization of one for the A exciton, while the polarization anisotropy is much smaller for the B and C excitons (cf. Figure 5. 4(b)).

The in-plane polarization anisotropy can be enhanced by anisotropic strain. This can be achieved by choosing a nonpolar orientation with an appropriate substrate. In the extreme case of m-plane GaN on $LiAlO_2$, the degree of linear polarization can be increased to its maximum value of one for all three transitions between the three uppermost valence bands (VBs) and the conduction band (CB), corresponding to complete linear polarization for all three transitions. This optical anisotropy can be observed in transmission (absorption) and reflection, as well as photoluminescence (PL) and photoreflectance (PR) spectroscopy. For

anisotropically strained C-plane GaN films on (11-20) sapphire, the in-plane polarization properties have been previously reported in Refs. [3-5].

The electrical and optical properties of semiconductors are mainly governed by the electronic band structure (EBS) in the vicinity of the absolute VB maximum and CB minimum. In heteroepitaxial layers, the EBS of the film material can be strongly modified because of strain induced by the mismatch of the lattice constants as well as the thermal expansion coefficients between the film and substrate. To correctly predict the optical transition energies and polarization properties of the strained film, it is important to determine the dependence of the EBS modification on in-plane strain [6].

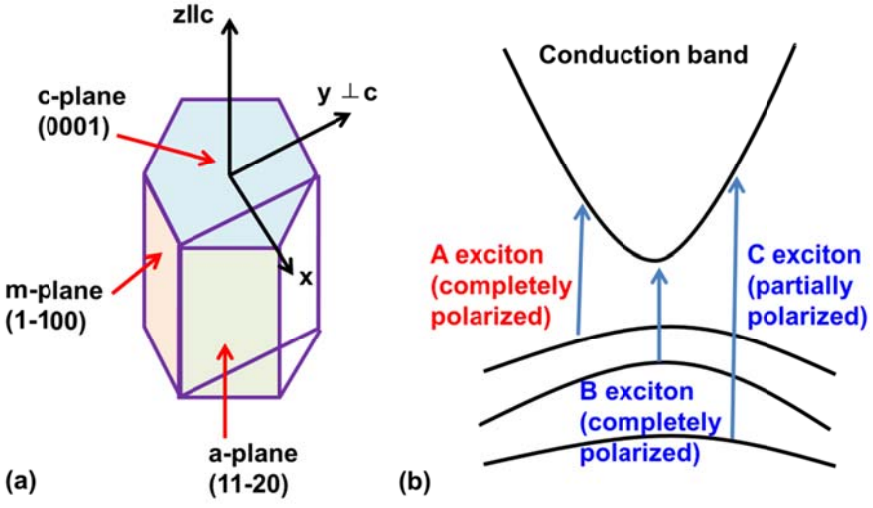

Fig. 5. 4 (a) The wurtzite unit cell of GaN showing the c-, m-, a-planes and the choice of coordinates. (b) Schematic electronic band structure (EBS) of unstrained GaN, showing the conduction band (CB) and valence bands (VBs) wave function symmetries. [6]

We found that light emitted from CIS a-plane GaN LED has the reduced polarization property. To confirm the reduced polarization property by silica nano-spheres, we experimentally measured the polarization ratio of top-emitted light of CIS a-plane GaN LED and performed three dimensional (3-D) finite-difference time-domain (FDTD) simulations.

First, we obtained the polarization ratio from top-emitted light of CIS a-plane GaN LED by measuring EL intensity on polarizer angle as shown in Fig. 5. 5. EL intensities of $E \perp c$ (m-direction) and E//c (c-direction) were also measured to calculate the polarization ratio. Definition of polarization ratio, ρ is $(I_{E \perp c} - I_{E//c})/ (I_{E \perp c} + I_{E//c})$ shown in Fig. 5. 5. I is normalized EL intensity. Polarization ratios of the CIS a-plane LED and the reference sample without silica nano-sphere were 0.27 and 0.59, respectively. Polarization ratio of CIS a-plane LED decreased by 0.32, compared to the value of a-plane LED without silica spheres.

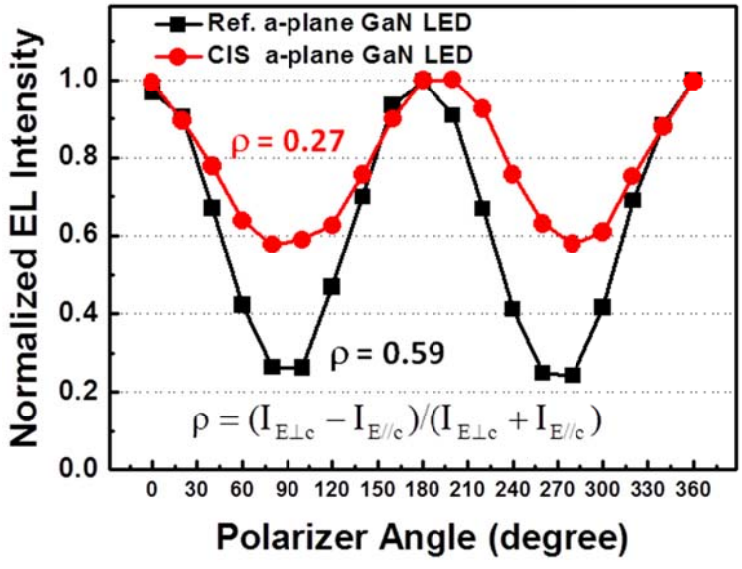

Fig. 5. 5 EL intensity of CIS a-plane GaN LED and reference a-plane GaN LED with polarizer angle from 0 to 360^{o}.

In order to confirm the effects of polarization conversion by silica nano-spheres, we performed the 3-D FDTD simulation. Polarization ratio of a-plane GaN LED with silica nano-spheres was calculated. Simulation model is shown in the inset of Fig. 5. 6.

We assumed a simple structure made of a GaN layer with height of 1 μm on sapphire substrate. A layer of periodic silica nano-spheres with diameter of 250 nm was on the sapphire substrate. Refractive index of GaN, silica and sapphire assumed 2.47, 1.46, 1.78, respectively at wavelength of 480 nm. Size of model is 3 μm × 3 μm. A perfectly matched layer (PML) boundary condition [7] was employed as absorbing boundary at top and bottom site of simulation region. Then, periodic boundary condition was employed along the four lateral boundaries to ignore the finite size of simulation model and assume the periodic structure of regular silica nano-sphere array. Mesh size is one tenth of the wavelength. To calculate accurately, mesh size of sphere lied section of simulation region was applied as 15 nm. Simulation time was 2000 fs.. A polarized dipole source along the E//c direction with wavelength of 480 nm was placed in the active layer Dipole source is located 300 nm beneath the surface of structure. Monitor that detects transmission of light is 350 nm above the surface of structure. We obtained total transmission of polarized emitted light along the $E \perp c$ and

E//c directions for calculation of polarization ratio. Surface coverage of silica nano-spheres was varied from 0 to 44.2 %.

The calculated result is shown in Fig. 5. 7. As the surface coverage increased from 0 to 44.2 %, the polarization ratio was decreased from 1.0 to 0.30. Each silica nano-sphere acts as a scattering center which changes direction of oscillation in electromagnetic wave. Therefore, polarization ratio decreases with increased surface coverage by silica nano-spheres. Calculated polarization ratio is similar to the experimental result for the sample with surface coverage of around 40%. We estimated that the silica nano-spheres with diameter of 250 nm act as the scattering center of polarized light emitted from the QW layer. Therefore the polarization property of emitted light was converted to the random orientations which cause the reduced polarization of EL emission of CIS a-plane GaN LEDs.

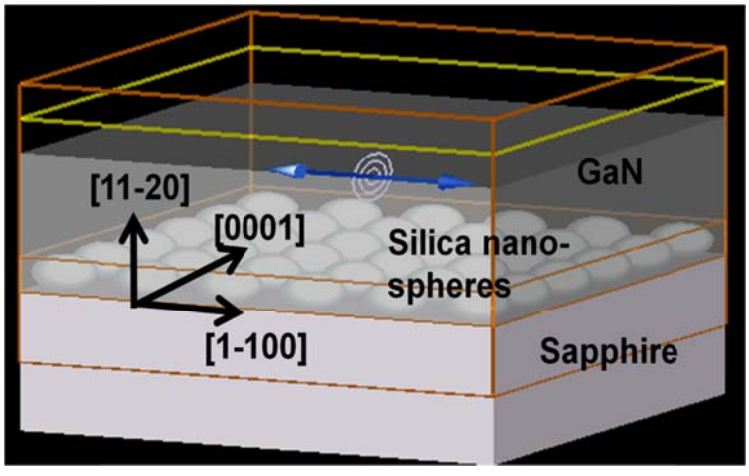

Fig. 5. 6 3D-FDTD simulation model of CIS a-plane GaN

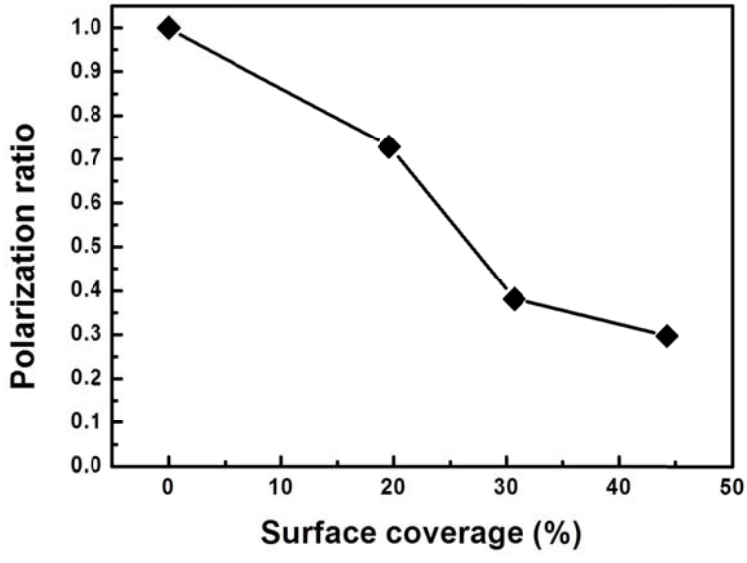

Fig. 5. 7 3D-FDTD simulation results of polarization ratio variation with surface coverage of silica nano-spheres in a-plane GaN layer grown on sapphire substrate.

5.5. Electrical properties of CIS a-plane GaN LED

We investigated the current-voltage (I-V) characteristics of the CIS a-plane GaN LED and reference LED. The forward voltage and series resistance of the CIS a-plane GaN LED were measured to be 3.65 V at 20 mA and 16.5 Ω, whereas those of the reference LED are 4.25 V at 20 mA and 20.5 Ω, respectively, as shown in Fig. 5. 8. The lower forward voltage and series resistance of the CIS a-plane GaN LED can be attributed to the improved crystal quality in less defective overgrown region of the CIS a-plane GaN template, which is similar to the result obtained for the conventional ELO a-plane GaN template [8].

To further investigate the forward voltage difference of CIS a-plane GaN LED and reference a-plane GaN LED, we first estimated that the band gap differences between CIS a-plane GaN and reference a-plane GaN. The optical energy gaps (Eg) of CIS a-plane and reference a-plane GaN were determined from Tauc's expression [9] for direct band gap semiconductor by linear extrapolation of the plot of $(\alpha h\nu)^2$ versus $h\nu$ to the energy axis. The physical bais fo Tauc's expression is the assumption of parabolic energy bands, an energy-dependent momentum matrix element and relaxation of momentum conservation. Fig. 5. 9 show the variation in the plot of $(\alpha h\nu)^2$

versus hν (Tauc's plot) for the CIS a-plane GaN and reference a-plane GaN. It was found that the calculated optical energy gap values were 3.39 eV for CIS a-plane GaN and 3.41 eV for reference a-plane GaN. This negligible bandgap difference could not be a major reason for the forward voltage difference between CIS a-plane GaN LED and reference a-plane GaN LED.

To investigate the strain state of these two a-plane samples, we measured the polarized Raman spectra [10-13]. Since strain states of CIS a-plane GaN and reference a-plane GaN measured by Raman spectra of A_1 (TO) and E_2 (high) as shown in Fig. 5. 10 were almost similar for CIS and ref. a-plane GaN (measurement step interval = 0.3 cm^{-1}), we confirmed that the negligible Raman shift originated from the similar strain state of CIS a-plane GaN and reference a-plane GaN.

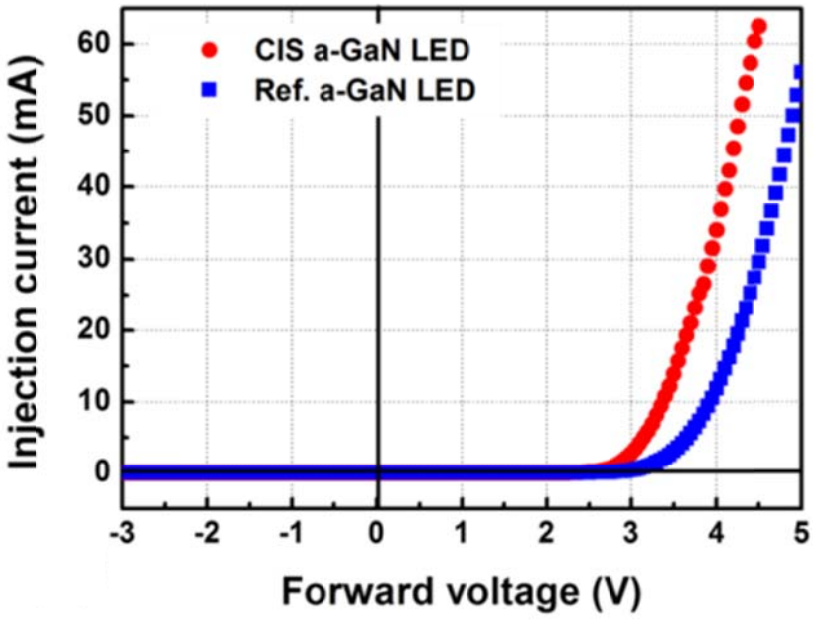

Fig. 5. 8 Current-voltage characteristics of CIS a-plane GaN LED and reference LED.

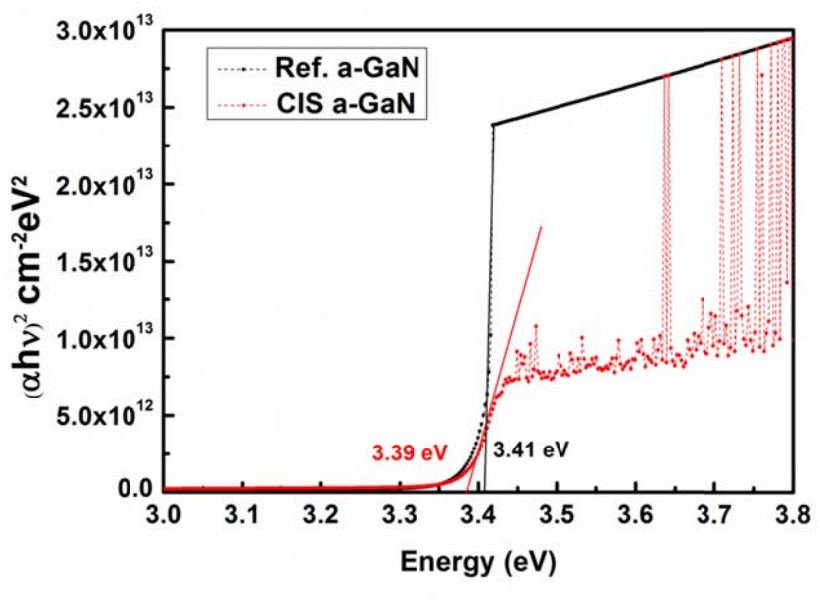

Fig. 5. 9 Optical energy gap for CIS a-plane GaN and reference a-plane GaN

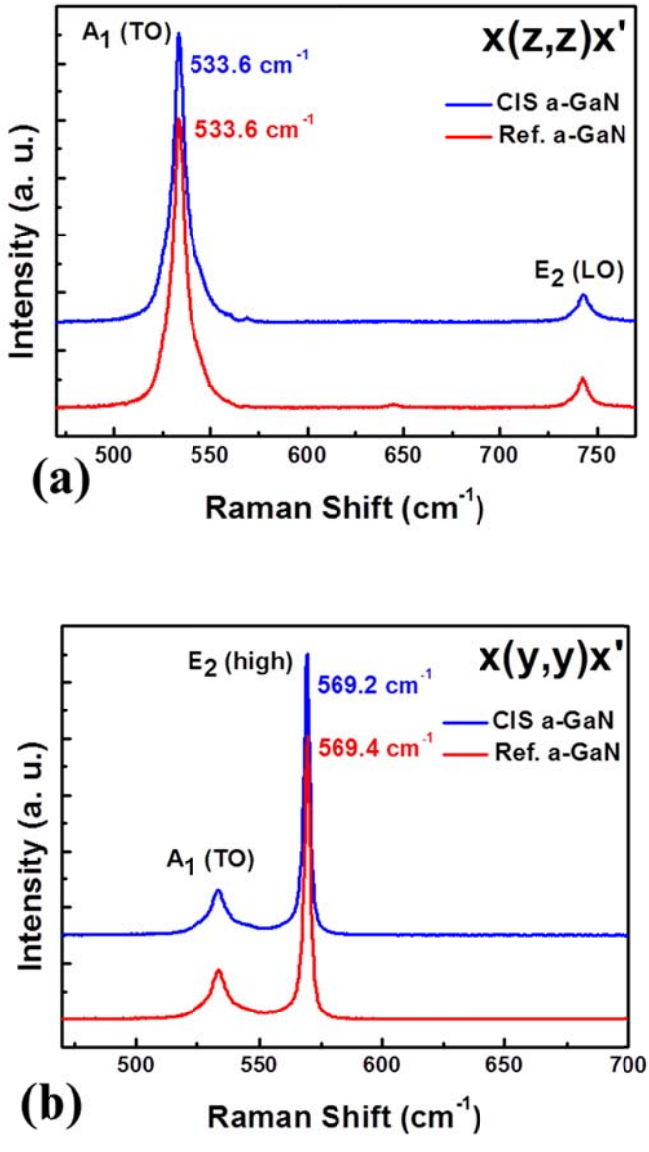

Fig. 5. 10 Polarized Raman spectra of CIS a-plane GaN and reference a-plane GaN. (a) x(z,z)x' and (b) x(y,y)x' are the scattering configuration.

Figure 5. 11 show the forward I-V curve of reference a-plane GaN LED and CIS a-plane GaN LED replotted in semilogarithmic scale of Fig. 5. 8. The I-V curves can be roughly divided into three regions [14, 15]: region I for the forward bias voltage less than 1.5 V, region II for the voltage between 1.5 and 3 V, and region III for the voltage larger than 3 V. The measured I-V characteristics can be understood in the following manner. GaN has extremely low intrinsic carrier concentrations at room temperature [14]. Since carrier concentration in the depletion region is almost zero, the excess current in region I is due to carrier recombination in depletion regions through trap levels presumably associated with threading defects such as dislocations and stacking faults in a-plane GaN [16]. Region II is well explained in terms of the ideal diode equation for p-n junctions assuming diffusion current. Since I-V curves suffer from Ohmic loss by bulk resistance at high bias voltage [17], the diode current is basically limited by series resistance as shown in Fig. 5. 8 and 5. 11, which indicated that the two LEDs had similar series resistance.

Although the two LEDs show the similar series resistance, reference a-plane LED exhibits larger leakage current than CIS a-plane GaN LED in region I. Those current were sufficiently high to involve a strong density of electronic localized states in the energy band gap in GaN, due to

the presence of defects such as impurities, vacancies, dislocations and stacking faults. Since the dislocation and stacking faults density of CIS a-plane GaN were lower than those of reference a-plane GaN, slight larger forward leakage current of reference a-plane GaN LED was observed in region I.

It is noted that as the leakage current is enhanced, the ideality factor increases and that a large ideality factor is often reported in GaN-based p-n junction diodes [18, 19]. Since the Ideal of dislocation and BSF in reference a-plane GaN LED increase the ideality factor of LED, the slope of I-V curve decrease and resulted in the forward voltage difference of two LEDs.

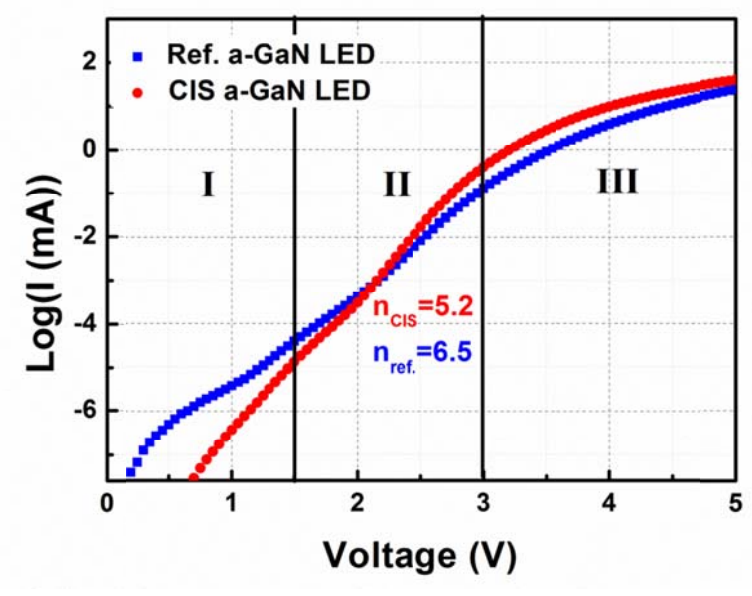

Fig. 5. 11 The forward I-V curve of reference a-plane GaN LED and CIS a-plane GaN LED replotted in semilogarithmic scale of Fig. 5. 8.

5.6. Light output power of CIS a-plane GaN LED

The dependences of the EL output power on the drive current tested on-wafer for the CIS a-plane GaN LED and a-plane GaN LED without silica nano-spheres in the layer are shown in Fig. 5. 12. The emission spectra were measured by a photo detector at drive currents ranging from 2 to 100 mA. The photo current generated from the CIS a-plane GaN LED shows a 150 ~ 130 % increase compared to that of the a-plane GaN LED without silica nano-spheres in the layer at the drive currents used in this test. We thus attribute the improved output power for the a-plane GaN LEDs to the decreased defect density in the GaN and increased extraction efficiency of the a-plane LED fabricated by the CIS process.

The dependence of EL output power on the input power for the CIS a-plane GaN LED and a-plane GaN LED without silica nano-spheres in the layer are shown in Fig. 5. 13. Output power of CIS a-GaN LED with input power shows a 180 ~165 % increase compared to that of the ref. LED. Electrical efficiency improvement of CIS a-plane GaN LED shows the less electrical loss to heating due to the less defective region of CIS a-plane GaN template.

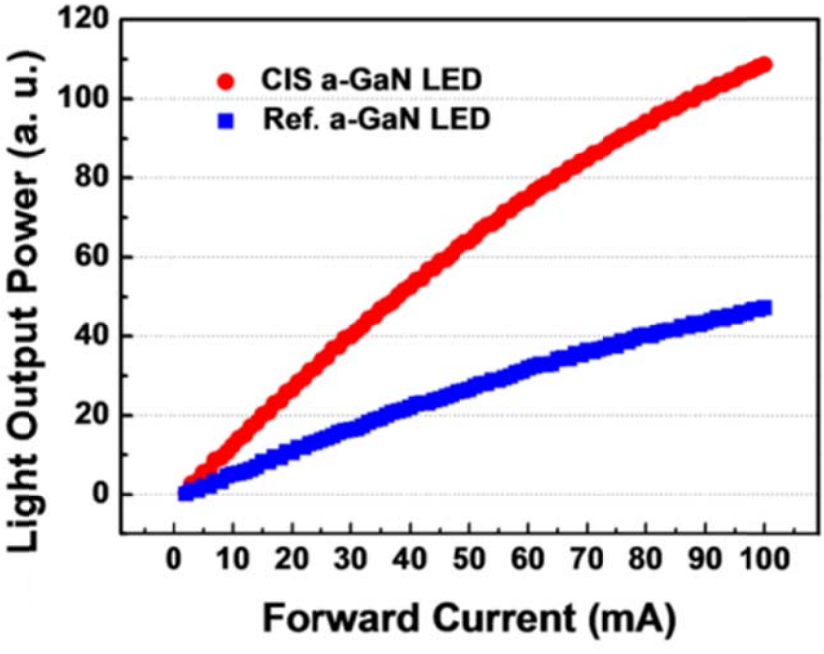

Fig. 5. 12 Light output power from the CIS a-plane GaN LED and reference a-plane GaN LED with injection currents in the range from 2 mA to 100 mA measured by a photodetector.

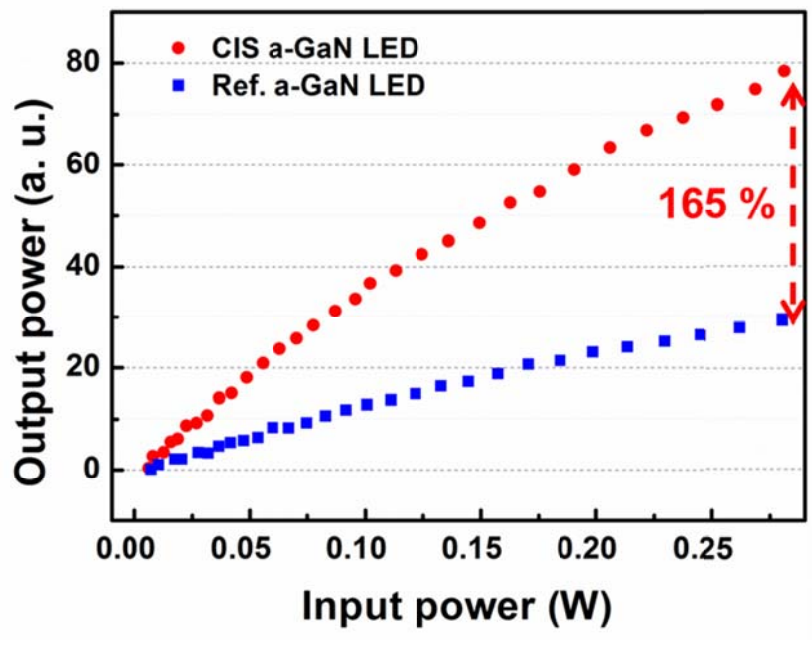

Fig. 5. 13 Light output power from the CIS a-plane GaN LED and reference a-plane GaN LED with input power.

5.7. Conclusion

In conclusion, a novel, simple and inexpensive efficiency improvement technique of LEDs employing silica nano-spheres is proposed. The silica nano-spheres were used as the mask layer for the regrowth of nonpolar a-plane GaN with reduced threading dislocation density and improved light extraction by the scattering process. Also, the silica nano-spheres in the GaN layer reduced the anisotropic optical polarization property of non-polar a-plane GaN. We expect that the optimization of the CIS growth process on nonpolar GaN will lead to further improvements, such as the lowering of the extended defect density and improvement of the extraction efficiency of nonpolar LEDs. In addition, the CIS technique could be extended to the growth of other mismatched hetero-epitaxial systems.

5.8. References

[1] S. H. Park, J. Park, D.-J. You, K. Joo, J. Jang, D.-U. Kim, H. Chang, S. Moon, Y.-K. Song, G.-D. Lee, H. Jeon, J. Xu, Y. Nanishi, and E. Yoon, Appl. Phys. Lett. 100, 191116 (2012)

[2] M. Funato, M. Ueda, Y. Kawakami, Y. Narukawa, T. Kosugi, M. Takahashi and T. Mukai, Jpn. J. Appl. Phys. 45, 26, L659 (2006).

[3] A. Alemu, B. Gil, M. Julier, and S. Nakamura, Phy. Rev. B, 57, 3761 (1998)

[4] M. Julier, J. Campo, J. B. Gil, et al. Phys. Rev. B 57, R 6791 (1998)

[5] P. P. Paskov, T. Paskova, P. O. Holtz, and B. Monemar, Phys. Stat. Sol. A, 190, 75 (2002)

[6] T. Paskova, "Nitride with Nonpolar Surface", Willy-VCH, pp 155-182 (2008)

[7] J.-P. Berenger, "A Perfectly Matched Layer for the Absorption of Electromagnetic Waves", Journal of Computational Physics, 114, 185, (1994)

[8] A. Chakraborty, B. A. Haskell, S. Keller, J. S. Speck, S. P. DenBaars, S. Nakamura, and U. K. Mishra, Appl. Phys. Lett. 85, 5143 (2004).

[9] J. Tauc, R. Grigorovici and A. Vancu, phys. Stat. sol. 15, 627 (1966)

[10] C. A. Arguello, D. L. Rousseau and S. P. Porto, Phys. Rev. 181, 1351 (1969)

[11] N. G. Weimann, L. F. Eastman, D. Doppulapudi, H. M. Ng, and T. D. Moustakas, J. Appl. Phys. 83, 3656 (1998)

[12] R. J. Briggs, A. K. Ramdas, Phys. Rev. B. 13, 5518 (1976)

[13] V. Darakchieva, T. Paskova, M. Schubert, H. Arwin, P. P. Paskov, B. Monemar, D. Hommel, M. Heuken, J. Off, F. Schiolz, B. A. Haskell, P. T. Fini, J. S. Speck, and S. Nakamura Phys. Rev. B 75, 195217 (2007)

[14] S. W. Lee, D. C. Oh, H. Goto, J. S. Ha, H. J. Lee, T. Hanada, M. W. Cho, T. Yao, S. K. Hong, H. Y. Lee, S. R. Cho, J. W. Choi, J. H. Choi, J. H. Jang, J. E. Shin and J. S. Lee, Appl. Phys. Lett., 89, 132117 (2006)

[15] L. Hirsch and A. S. Barriere, J. Appl. Phys., 94, 5014 (2003)

[16] Z. Z. Bandic, P. M. Bridger, E. C. Piquette, and T. C. McGill, Appl. Phys. Lett., 72, 3166 (1998)

[17] Neudeck and R. F. Pierret , “The PN Junction Diode, Modular Series on Solid State Devices”, Addison-Wesley, Reading, MA, Vol. III, pp. 45-91 (1989)

[18] L. Hirsch and A. S. Barriere, J. Appl. Phys., 94, 5014 (2003)

[19] K. Mayes, A. Yasan, R. McClintock, D. Shiell, S. R. Darvish, P. Kung, and M. Razeghi, Appl. Phys. Lett. 84, 1046 (2004)

Chapter 6. Growth of a-plane GaN with nano-voids integrated into buffer layer

6.1. Introduction

Wurtzite GaN-based light emitting diode (LED) structures grown along the c-axis suffer from strong polarization related to internal electric fields, which induce the spatial separation of electrons and holes in the active layers and a resulting red-shift of the emission wavelength due to the quantum confined Stark effect [1]. To prevent these adverse effects, several groups have tried to grow GaN-based LED structures on nonpolar planes, such as the a-plane or m-plane [2,3]. To achieve high efficiency nonpolar LEDs for general illumination, the development of high quality nonpolar GaN epitaxial layers with a low defect density and a cost-effective technique to improve the light extraction efficiency of LEDs are required.

Although nonpolar GaN substrates with high crystallinity can be obtained by slicing a thick c-plane GaN wafer grown by hydride vapor phase epitaxy (HVPE),[4] $(1\bar{1}02)$ r-plane sapphire is still the most commonly used large-area substrate for a-plane GaN growth, due to its relatively low cost.

However, the major drawback of r-plane sapphire substrates for the

growth of nonpolar a-plane GaN is the high defect density in the a-plane GaN epitaxial layer. These defects mainly originate from the 16 % difference in the lattice constants between a-plane GaN and r-plane sapphire along the m-direction of GaN, resulting in high density, non-radiative recombination centers in a-plane GaN LEDs [3]. In addition, the enhanced in-plane growth rate anisotropy of a-plane GaN on r-plane sapphire results in the 3-dimensional (3D) growth of a-plane GaN. This 3D growth leaves a large number of micrometer-scale triangular pits on the GaN surface during the coalescence of the islands [3,5,6].

To prevent the formation of rough surfaces and/or triangular pits in a-plane GaN, most research groups have tried to grow nonpolar GaN at relatively low pressures to enhance the formation of islands in the nucleation layer [5-8]. This growth condition facilitated the coalescence of a-plane GaN at the early stage of growth, leading to pit-free surfaces. However, the coalesced surface formed at low pressure is usually grown at the expense of numerous threading dislocations in the epitaxial layer, due to the increased number of islands formed during its growth. To improve the crystalline quality of a-plane GaN, several research groups have reported the use of conventional epitaxial lateral overgrowth (ELO) or a modified ELO process on top of low-pressure-grown a-plane GaN with high threading dislocation

density [9-11]. However, such ELO processes resulted in long processing times and, hence, high cost, due to the complexity of such processes as mask deposition and etching.

In order to improve the emission efficiency of nonpolar a-plane GaN light emitting diodes (LEDs) by a simple process, we have reported that the controlled integration of silica nano-spheres (CIS) into the a-plane GaN epitaxial layer grown on r-plane sapphire by metal-organic chemical vapor deposition [12]. In this CIS process, the silica nano-spheres integrated in the valley act as SiO_2 mask layers in the subsequent epitaxial lateral overgrowth (ELO) process. In addition to the ELO effect by the silica nano-spheres, the silica nano-spheres integrated in the GaN can improve the light extraction efficiency (LEE) of GaN-based LEDs. Nanometer-scale stacked silica spheres act as internal scattering centers of the light emitted from the active layer of the LEDs. This internal light scattering changes the path of the emitted light to the top surface of LEDs. Therefore, the LEE of CIS GaN-based LEDs are increased by the enhanced probability of entering escape cone defined by the critical angle for total internal reflection.

In this experiment, we proposed the nano-viods in the a-plane GaN layers. Similar to the CIS a-plane GaN layer, integrated nano-voids in the a-plane GaN layer improved the crystalline quality of a-plane GaN

subsequently grown on void due to the ELO process. In addition to the crystalline quality improvement, nanometer-scale spherical-shaped voids act as internal scattering centers of the light emitted from the active layer of the LEDs. This internal light scattering changes the path of the emitted light to the top surface of LEDs. Since the scattering of light enhanced when the refractive index difference between GaN (n=2.43) and scattering center such as silica nano-sphere (n=1.46) or nano-voids (n=1) is larger, scattering in the GaN layer will be increase by using nano-voids compared to the silica nano-spheres. Therefore, the LEE of nano-voids a-plane GaN LEDs are increased compared to that of CIS a-plane LED.

Due to the large thermal expansion coefficient difference between GaN and sapphire, heteroepitaxial GaN layer grown on sapphire suffer from the compressive stress and wafer bowing [13]. In case of nonpolar GaN on sapphire substrate, anisotropic material properties in the growth plane resulted in the anisotropic strain in the layer. Integrated nano-air voids near the GaN and sapphire interface compensate the internal strain of epitaxial layers [14], therefore nano-voids will decrease the compressive strain in the epitaxial layer which resulted in the reduction of wafer bowing.

6.2. Experimental procedure

r-plane sapphire wafers (-0.2 ± 0.05^{o} off toward the m-axis of sapphire) were used as the substrates. The entire growth process for the nano-voids a-plane GaN was performed using a Thomas Swan 3 x 2 inch MOCVD reactor with hydrogen as a carrier gas and trimethylgallium and ammonia as precursors in the GaN growth process. The 3D-shaped a-plane GaN buffer layer was grown at a pressure of 300 torr. The controlled integration of the silica nano-spheres on the 3D a-plane GaN layer was performed using a spin coating method. The silica nano-spheres used in this experiment were dispersed in ethanol solution and their average diameter was 250 nm. For the fabrication of templates of nano-voids a-plane, regrowth was performed for 10 min to fill the gap between the silica nano-spheres. Then the remained silica nano-spheres were etched by hydrogen fluoride (HF) to form the spherical nano-viods in the a-plane GaN template. For the overgrowth step on the silica nano-spheres, the growth pressure was decreased to 100 torr to promote the lateral growth of GaN. For the growth process, the V/III ratio and growth temperature were maintained at 380 and 1040 ^{o}C, respectively.

6.3. Fabrication of nano-voids in the a-plane GaN layers

On r-plane sapphire, we intentionally fabricated a rough a-plane GaN buffer layer by metal-organic chemical vapor deposition (MOCVD) and selectively masked trench areas with silica nano-spheres. After the 10 min GaN regrowth on this template, some part of the gap between silica nano-spheres were filled by GaN. From the chemical etching by hydrogen fluoride (HF), silica nano-spheres were etched and integrated spherical nano-voids were remained. During subsequent regrowth process, the nano-voids were not easily filled by GaN due to the selectivity of GaN growth process. The nano-voids blocked the propagation of the threading dislocations originating at the interface between the GaN and the sapphire substrate. In this study, we utilized the previously reported CIS process to form the spherical shaped nano-voids.

A schematic of the formation of nano-voids in the a-plane GaN and regrowth process is illustrated in Fig. 6. 1.

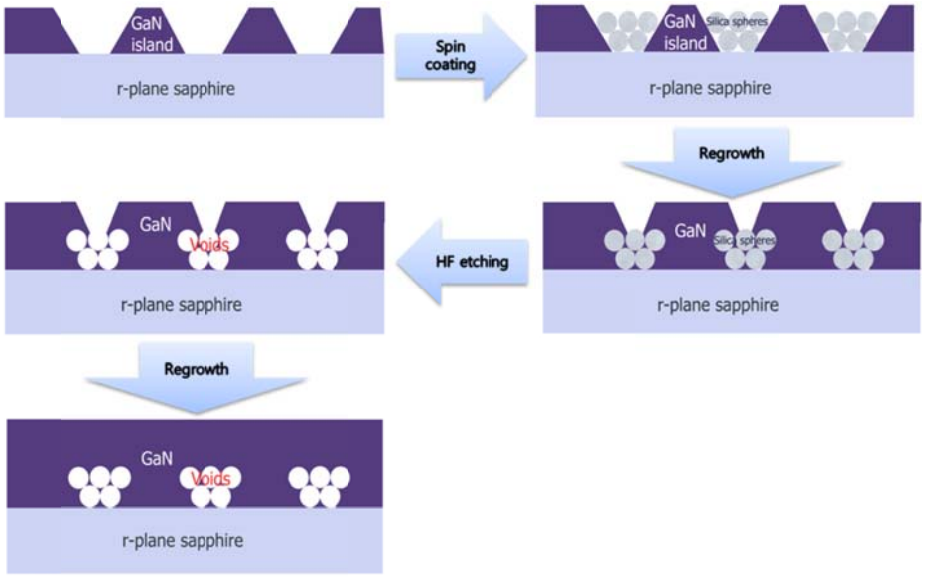

Fig. 6. 1 Scheme of the nano-voids formation in a-plane GaN layer. : 3D-shaped a-plane GaN buffer; controlled integration of silica nano-spheres on 3D-shaped a-plane GaN buffer; regrowth of a-plane GaN for 10 min; lateral overgrowth of GaN on the integrated nano-voids; full coalescence of the a-plane GaN with nano-voids.

A 3D-shaped a-plane GaN buffer layer (1-μm-thick) with various facets such as $\{1\bar{1}01\}$ and $(000\bar{1})$ was grown, as shown in Fig. 6. 2(a). Then, silica nano-spheres with a diameter of 250 nm were preferentially integrated in the trench area of the 3D buffer layers by using a conventional spin coating method. The silica nano-spheres from an aqueous colloidal suspension were spread out on the substrate and integrated into the trench areas of the 3D GaN layer by evaporating the solution and subsequently displacing the silica nano-spheres to the trench area during the spin coating process [15-17]. Fig. 6. 2(b) shows a scanning electron microscopy (SEM) image of the a-plane GaN buffer layer with silica nano-spheres integrated in the trench area. During the 10 min GaN regrowth on this CIS GaN buffer layer at high temperature, the gap between silica nano-spheres were filled by GaN as shown in Fig. 6. 3.

Figure 6. 4 shows the spherical nano-voids in the a-plane GaN layer. From the chemical etching by HF, silica nano-spheres were etched and we can observe the spherical shaped nano-voids in the site where the silica nano-sphere exist before the HF chemical etching. Nano-voids in the trenches of the 3D shaped a-plane GaN buffer layer, act as a mask for the subsequent ELO process.

Fig. 6. 5 shows a cross-section SEM image of the a-plane GaN after

formation of nano-voids in the layer and regrowth process. The laterally grown a-plane GaN epitaxial layers on the integrated nano-voids are fully coalesced without the triangular pits commonly observed in the surface of the a-plane GaN.

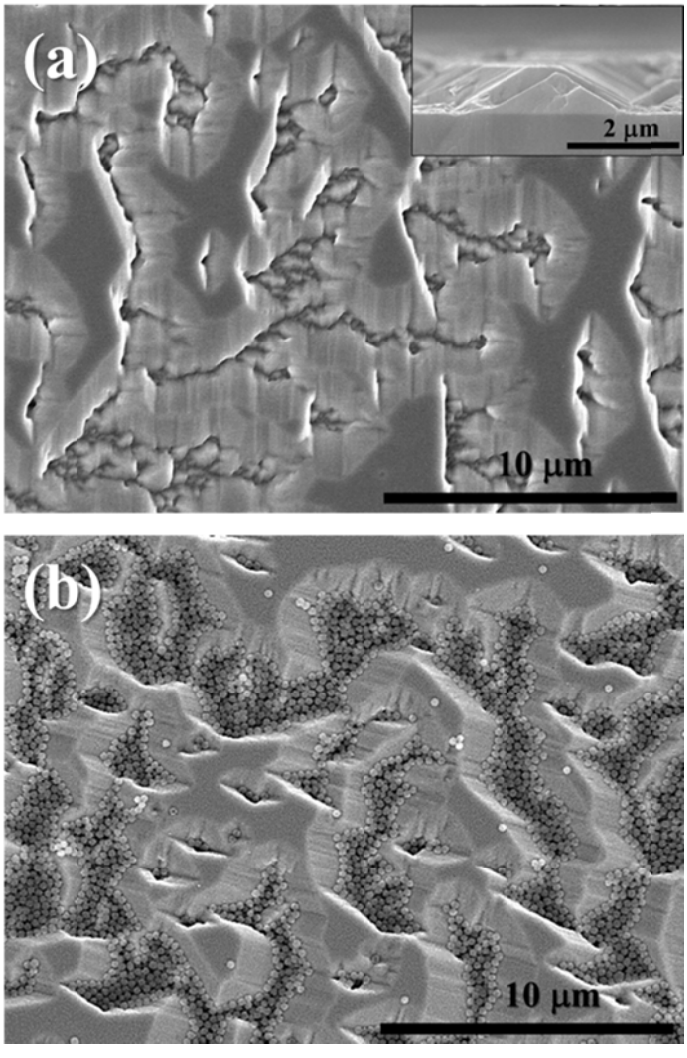

Fig. 6. 2 (a) SEM image of 3D-shaped a-plane GaN buffer. Inset: cross-section SEM image of GaN buffer. (b) SEM image of controlled integration of silica nano-spheres on 3D-shaped a-plane GaN buffer by spin coating method.

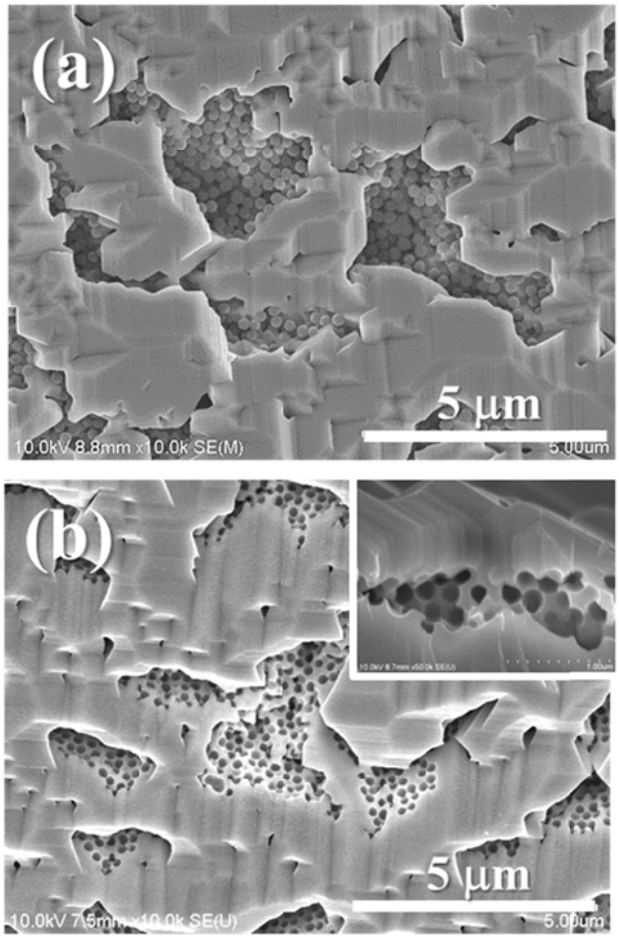

Fig. 6. 3 (a) SEM image after 10 min regrowth of a-plane GaN on CIS template. (b) spherical nano-voids in the a-plane GaN template after HF etching.

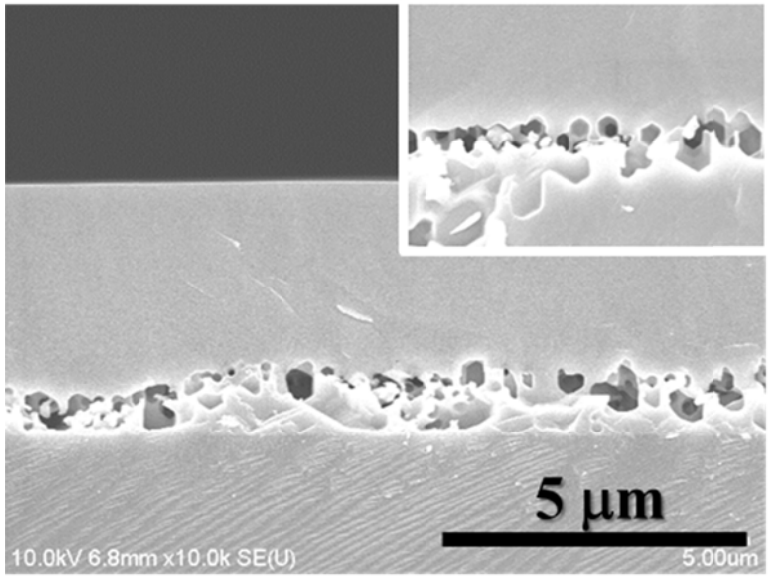

Fig. 6. 4 Cross-section SEM image of full coalescence of a-plane GaN with embedded nano-voids.

6.4. FDTD simulations of a-plane GaN with embedded nano-structures

To confirm the effect of spherical shaped nano-voids on light extraction efficiency of LEDs, we performed three dimensional (3-D) finite-difference time-domain (FDTD) simulations.

First, we assumed a simple 2D structure of single nano-spheres sphere with different refractive index from 1 to 2.2 in the GaN matrix (n=2.43). We obtained the qualitative results of light scattering by nano-spheres as shown in Fig. 6. 5. As the refractive index of nano-sphere was increased, the light scattering by nano-sphere in the GaN matrix was increased.

To investigate the effect of nano-voids on the light extraction efficiency of LEDs, we assumed a simple structure made of a GaN layer with height of 2.3 μm on sapphire substrate. A layer of stacked nano-spheres with diameter of 250 nm, stacked nano-voids and SiO_2 mask were on the sapphire substrate as shown in Fig. 6. 6. Surface coverage of nano-spheres was about 40 %.

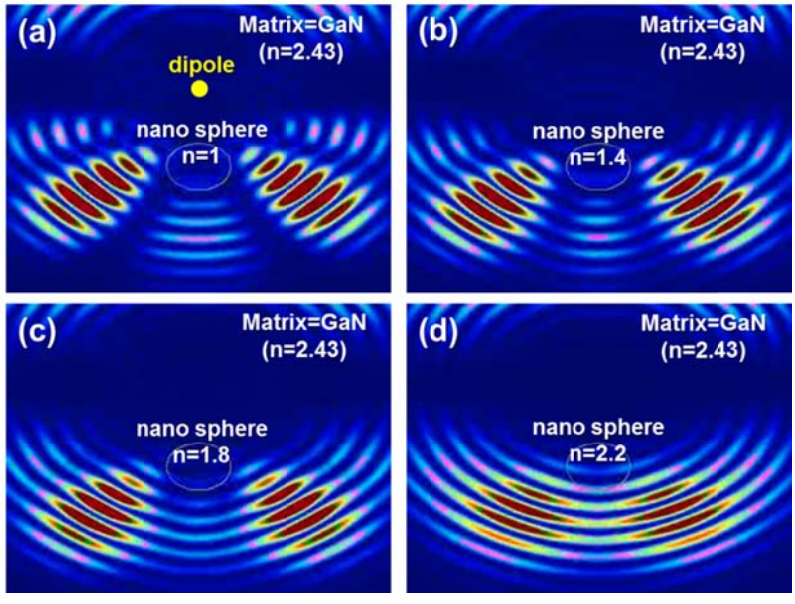

Fig. 6. 5 2D FDTD simulations of light scattering by nano-sphere with different refractive index of (a) n=1; air, (b) n=1.4; silica, (c) n=1.8 and (d) n=2.2. The matrix material of simulation was GaN with n=2.43.

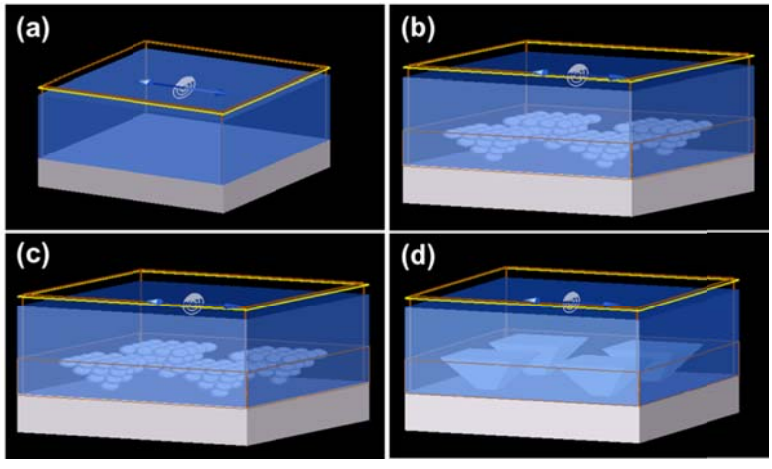

Fig. 6. 6 3D-FDTD simulation models of LEDs with embedded nano-structure. (a) reference, (b) LED with stacked silica nano-spheres, (c) LED with stacked air-spheres and (d) LED with SiO_2 mask

Refractive index of GaN, silica and sapphire assumed 2.47, 1.46, 1.78, respectively at wavelength of 480 nm. Size of model is 3.2 μm × 3.2 μm. A perfectly matched layer (PML) boundary condition [18] was employed as absorbing boundary at top and bottom site of simulation region. Then, periodic boundary condition was employed along the four lateral boundaries to ignore the finite size of simulation model and assume the periodic structure of regular silica nano-sphere array. Mesh size is one tenth of the wavelength. To calculate accurately, mesh size of sphere lied section of simulation region was applied as 15 nm. Dipole source is located 100 nm beneath the surface of structure. Monitor that detects transmission of light is 350 nm above the surface of structure. We obtained total emission to the top surface to calculate extraction efficiency of the structures.

The calculated results are shown in Fig. 6. 7. The extraction efficiency of LEDs with embedded structures show the 60 to 160 % higher than that of reference LED without structure in the layer.

Especially, spherical shaped stacked nano-spheres show the much higher extraction efficiency than the GaN with SiO_2 mask due to the scattering effect by nanoscale particles. Also, LED with stacked nano-voids shows the 20 % higher extraction efficiency than LED with stacked silica nano-spheres due to the refractive index difference between silica (n=1.46)

and air (n=1).

We estimated that the scattering in the GaN layer will be increase by using nano-voids compared to the silica nano-spheres. Therefore, the LEE of nano-voids a-plane GaN LEDs will increase compared to that of CIS a-plane LED.

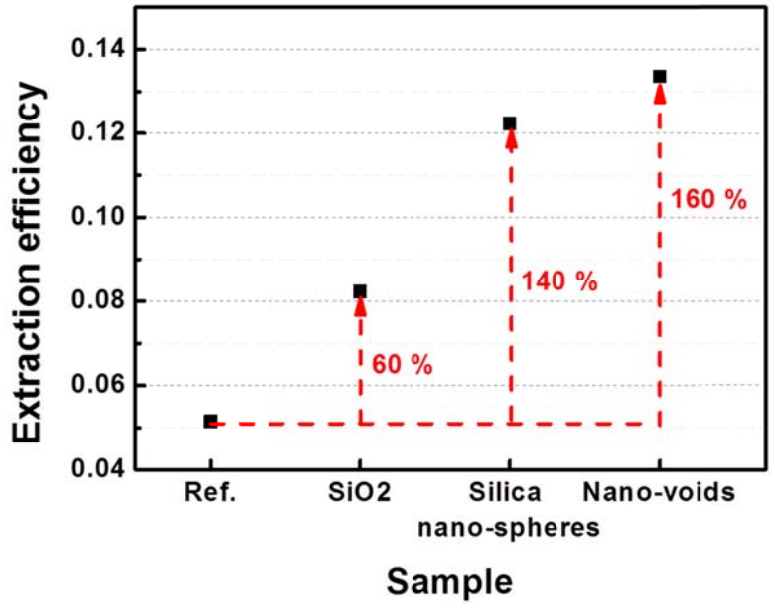

Fig. 6. 7 3D FDTD simulation results of extraction efficiency of LEDs with different embedded structures.

6.5. Conclusion

In conclusion, a novel, simple and inexpensive efficiency improvement technique of LEDs employing nano-air voids is proposed. The silica nano-spheres were used as the template for the formation of nano-voids and regrowth of nonpolar a-plane GaN. A-plane GaN with embedded nano-voids will improve the light extraction by the scattering process and reduce the wafer bowing by formation of voids at the interface of GaN and sapphire substrate. We expect that the optimization of the nano-voids formation and growth process on nonpolar GaN will lead to further improvements, such as the lowering of the extended defect density, improvement of the extraction efficiency and reduced compressive strain in the layer of nonpolar LEDs.

6.6. References

[1] D. A. B. Miller, D. S. Chemla, T. C. Damen, A. C. Gossard, W. Wiegmann, T. H. Wood and C. A. Burrus, Phys. Rev. Lett. 1984, 53, 2173.

[2] P. Waltereit, O. Brandt, A. Trampert, H. T. Grahn, J. Menniger, M. Ramsteiner, M. Reiche and K. H. Ploog, Nature 406, 865 (2000).

[3] M. D. Craven, S. H. Lim, F. Wu, J. S. Speck and S. P. DenBaars, Appl. Phys. Lett. 81, 469 (2002).

[4] K. C. Kim, M. C. Schmidt, H. Sato, F. Wu, N. Fellows, Z. Jia, M. Saito, S. Nakamura, S. P. DenBaars and J. S. Speck, Appl. Phys. Lett. 91, 181120 (2007).

[5] X. Ni, Y. Fu, Y. T. Moon, N. Biyikli, and H. Morkoç, J. Cryst. Growth 290, 166 (2006).

[6] Q. Sun, C. D. Yerino, T. S. Ko, Y. S. Cho, I.-H. Lee, J. Han and M. E. Coltrin, J. Appl. Phys., 104, 093523 (2008).

[7] T. S. Ko, T. C. Wang, R. C. Gao, H. G Chen, G. S. Huang, T.C. Lu, H. C. Kuo, J. Cryst. Growth, 300, 308 (2007).

[8] S.-N Lee, H. S. Paek, J. K. Son, T. Sakong, O. H. Nam, Y. Park , J. Cryst. Growth 307, 358 (2007).

[9] F. Wu, M. D. Craven, S. H. Lim, and J. S. Speck, J. Appl. Phys. 94, 942 (2003).

[10] Q. Li, Y. Lin, J. R. Creighton, J. J. Figiel and G. T. Wang, Adv. Mater. 21, 2416 (2009).

[11] D. Iida, M. Iwaya, S. Kamiyama, H. Amano and I. Akasaki, J. Cryst. Growth, 311, 2887 (2009).

[12] S. H. Park, J. Park, D.-J. You, K. Joo, J. Jang, D.-U. Kim, H. Chang, S. Moon, Y.-K. Song, G.-D. Lee, H. Jeon, J. Xu, Y. Nanishi, and E. Yoon, Appl. Phys. Lett. 100, 191116 (2012)

[13] Y. Kim, N. A. Shapiro, H. Feick, R. Armitage, and E. R. Weber, Appl. Phys. Lett. 78, 895 (2001)

[14] J. H. Kim et al., in preparation

[15] Y. Xia, Y. Yin, Y. Lu and J. McLellan, Adv. Funct. Mater. 13, 907 (2003).

[16] Y. Cui, M. T. Björk, J. A. Liddle, C. Sönnichsen, B. Boussert and A. P. Alivisatos, Nano Lett. 4, 1093 (2004).

[17] S. M. de Sousa Pereira, M. A. Martins, T. Trindade, I. M. Watson, D. Zhu and C. J. Humphreys, Adv. Mater. 20, 1038 (2008).

[18] J.-P. Berenger, Journal of Computational Physics 114, 185, (1994)

Chapter 7. Conclusion

In this study, for the high efficiency nonpolar a-plane GaN light emitting diode grown on r-plane sapphire substrate, high quality a-plane GaN templates are fabricated. The study starts from the growth of a-plane GaN buffer layers.

To obtain pit-free and improved crystal quality a-plane GaN by metal-organic chemical vapor deposition, we intentionally grew high-temperature (HT) 3-dimensional (3D) GaN buffer layers on a GaN nucleation layer. The effects of the HT 3D GaN buffer layers on crystal quality and the surface morphology of a-plane GaN were studied. The insertion of a 3D GaN buffer layer with an optimum thickness was found to be an effective method to obtain pit-free a-plane GaN with improved crystalline quality on r-plane sapphire substrates. An a-plane GaN light emitting diode (LED) at an emission wavelength around 480 nm with negligible peak shift was successfully fabricated.

We utilized the 3D growth nature of a-plane GaN and controlled integration of silica nano-spheres into the rough GaN buffer layer to improve the crystalline quality of nonpolar a-plane GaN. In addition to the crystalline quality improvement by silica nano-spheres, the silica nano-spheres

integrated in the GaN can improve the light extraction efficiency (LEE) of GaN-based light emitting diodes (LEDs). Nanometer-scale silica spheres act as internal scattering centers of the light emitted from the active layer of the LEDs. Thus, the angle of reflected light at the GaN/sapphire interface is distributed over a wide range of angles. Therefore, the LEE of GaN-based LEDs is increased by the enhanced probability of entering escape cone defined by the critical angle for total internal reflection. The light output power from the CIS a-plane GaN LEDs show a 130 ~ 150 % increase compared to that of the a-plane GaN LED without silica nano-spheres in the layer. We thus attribute the improved output power for the a-plane GaN LEDs to the decreased defect density in the GaN and increased extraction efficiency of the a-plane LED fabricated with silica nano-spheres.

And, we proposed the a-plane GaN with nano-viods integrated into a-plane GaN layers using CIS process. Similar to the CIS a-plane GaN layer, integrated nano-voids in the a-plane GaN layer improved the crystalline quality of a-plane GaN subsequently grown on void due to the ELO process. In addition to the crystalline quality improvement, nanometer-scale spherical-shaped voids act as internal scattering centers of the light emitted from the active layer of the LEDs. Since the scattering of light enhanced when the refractive index difference between GaN (n=2.43) and scattering

center such as silica nano-sphere (n=1.4) or nano-voids (n=1) is larger, scattering in the GaN layer will be increase by using nano-voids compared to the silica nano-spheres. Integrated nano-voids near the GaN and sapphire interface compensate the internal strain of epitaxial layers, therefore nano-voids will decrease the compressive strain in the epitaxial layer which resulted in the reduction of wafer bowing.

Until now, theoretical calculations show the nonpolar GaN based LEDs could be a candidate for a future high efficiency LEDs. The major obstacles for the application of nonpolar GaN were the high defects density and low light output power. In this study, we confirmed that the CIS and utilization of CIS techniques would be a solution for the high quality nonpolar a-plane GaN growth and high efficiency nonpolar GaN LEDs. And these techniques would be helpful to adopt the nonpolar GaN for the high efficiency future commercial LED. In addition, the CIS and utilization of CIS technique could be extended to the growth of other mismatched hetero-epitaxial systems.

국문초록

질화물 기반의 (0001)면 극성 기판에 성장된 이종에피구조는 자발 분극과 압전 분극으로부터 생기는 강력한 내부 전기장의 영향을 받게 된다. 이러한 내부 전기장은 양자우물 구조에서 전자와 정공의 공간적인 분리를 야기하여 효율을 감소시키고 quantum confined Stark effect 에 의해서 발광 파장의 적색 편이 현상이 발생하게 된다. 이러한 현상을 극복하기 위해서 여러 연구 그룹에서는 GaN 기반의 구조를 비극성 또는 반극성 면에 성장하는 노력을 하고 있다. 본 연구에서는 r면 사파이어 기판에 고효율의 비극성 a면 GaN 발광 다이오드를 성장하기 위해서 고품위의 a면 GaN을 성장하였다.

유기금속화학기상증착법을 이용하여 표면에 삼각형 형태의 피트가 형성되지 않고 결정성이 향상된 a면 GaN을 성장하기 위해서 의도적으로 3차원 형태의 버퍼층을 형성하였다. 그리고 3차원 형태의 버퍼층이 a면 GaN 의 결정성과 표면 형상에 미치는 영향을 연구하였다. 사파이어 기판 상에 a면 GaN을 성장할 때, 성장 속도의 이방성에 의해 발생되는 3차원 성장의 특성을 활용하여 3차원 형태의 버퍼층을 형성하였다. 3차원 형태의 버퍼층을 최적화된 두께로 에피층 성장 중간에 삽입하면 에피층의 관통전위 등의

결함을 측면성장방법을 통하여 감소시켜 결정성이 향상된 a면 GaN을 성장할 수 있다.

비극성 a면 GaN의 결정성을 더욱 향상시키고 발광 다이오드의 효율 증대를 위해서 앞서 거론된 3차원 형태로 성장되는 a면 GaN의 특성을 활용하였고, 이러한 3차원 형태의 버퍼층의 트렌치 부분에 실리카 나노 구를(silica nano-spheres) 채워 넣었다. 이러한 과정을 CIS(controlled integration of silica nano-spheres)라고 정의하였다. 이러한 트렌치 영역에 채워진 실리카 나노 구가 측면성장법의 마스크 층으로 작용하여 이 위에 a면 GaN 을 재성장 할 때 에피층의 결정성이 향상 된다. 또한 나노미터 크기의 실리카 구들이 발광 다이오드의 활성층에서 발생한 빛의 산란을 야기하여 GaN/사파이어 계면에서 산란된 빛들의 진행 각도가 광범위 하게 변하게 된다. 실리카 나노 구의 산란 효과로 인해서 에피층 외부로 나오게 되는 빛이 전반사를 위한 임계각 보다 작은 각도를 가지는 확률이 커지기 때문에 GaN 기반 발광 다이오드의 광 추출효율이 증가하게 된다. 실리카 나노 구를 이용한 비극성 CIS a면 GaN 발광다이오드는 실리카 구가 없는 발광다이오드에 비하여 광 출력이 130~150% 증가하였다. 이러한 광 출력의 증가는 실리카 나노 구의 삽입으로 인한 결함밀도 감소와 발광다이오드의 광 추출효율 향상에서 비롯된다.

앞서 이야기한 CIS 과정을 응용하여 a면 GaN 에피층 내부에 나노 공극(nano-voids)이 형성된 a면 GaN 을 성장하였다. CIS a면 GaN과 유사하게 에피층 내부에 존재하는 나노 공극은 공극 상단에서 측면성장 효과로 인해서 a면 GaN의 결정성을 향상시킨다. 결정성 향상뿐만 아니라 나노 공극의 굴절률은(n=1) 기존 실리카 구의 굴절률(n=1.4) 비해서 GaN 에피층의 굴절률(n=2.4)과 차이가 더 크기 때문에 실제 발광 다이오드를 제작할 때 광 추출효율도 실리카 구를 이용할 때 보다 더 증가할 수 있다. 또한 결정성 향상의 효과와 광 추출효율 향상의 효과 이외에도 기판과 에피층 사이의 계면에 형성된 나노 공극들로 인해서 에피성장 후 GaN 과 사파이어 기판의 열팽창 계수 차이에서 야기되는 기판 내부의 잔류응력 제거와 기판 휨 감소에도 효과적이다.

주요어:

비극성, a면 GaN, r면 사파이어, 발광다이오드, 유기금속화학기상증착법, 나노 구, 측면에피성장, 광 추출효율

학번:

2006-23048

Publication list

Journal Papers:

1. S. H. Park, J. Park, D.-J. You, K. Joo, D. Moon, J. Jang, D.-U. Kim, H. Chang, S. Moon, Y.-K. Song, G.-D. Lee, H. Jeon, J. M. Xu, Y. Nanishi and E. Yoon "Improved Emission Efficiency of a-plane GaN Light Emitting Diodes with Silica Nano-Spheres integrated into a-plane GaN Buffer Layer", Appl. Phys. Lett. 100, 191116 (2012).

2. S. H. Park, D. Moon, B. Kim, K. Joo, D.-J. You, D.-U. Kim, H. Jang, H. Jeon, Y. Nanishi and E. Yoon "Improved Crystal Quality of a-plane GaN with High- temperature 3-dimensional GaN Buffer Layers Deposited by Using Metal-organic Chemical Vapor Deposition", J. Korean Phys. Soc. 60, 1297 (2012)

3. S. H Park, J. Park, D. Moon, N. Kim, D.-J. You, J. Kim, J. Kang, S.-M. Lee, J.-S. Kim, M.-S. Yang, T. Kim and E. Yoon "Effects of r-plane Sapphire Substrate Tilt Angles on the Growth Behavior of Nonpolar a-plane GaN" J. Korean Phys. Soc. 58, 906 (2011)

4. K.-H. Lee, I. Shin, S. H. Park, D. Moon, M. H. Kim, J. Park, Y. Nanishi and E. Yoon "Growth of Less Bowed GaN Epitaxial Layers on Sapphire Substrates by Formation of Low-Temperature GaN Buffer Layer with Columnar Microstructure" Jpn. J. Appl. Phys. 51, 01AF01 (2012)

5. J. Park, D. Moon, M. H. Kim, S. H. Park and E. Yoon "Growth of GaN Branched a-Si_3N_4 Nanowires on (100) Si by Metal Organic Chemical

Vapor Deposition" Mater. Lett. (2012)

6. K.-H. Lee, S. H. Park, J. H. Kim, N. Kim, M. H. Kim, H. Na and E. Yoon, "MOCVD growth of GaN layer on InN interlayer and relaxation of residual strain" Thin Solid Films 518, 6365 (2010)

7. J. Park, K. H. Kim, S. H. Park, E. Yoon and T. Yao, "Catalyst-Free Growth of Vertically Aligned ZnO Nanostructures Arrays on Periodically Polarity-Inverted Substrate" Appl. Phys. Express 3, 105001 (2010)

8. J. Park, T. Goto, S. H. Park, J. Ha, E. Yoon and T. Yao, "Ultraviolet stimulated emission in periodically polarity-inverted ZnO structures at room temperature" Appl. Phys. Lett. 97, 171101 (2010)

9. J. Park, S.-I. Baik, D.-S. Ko, S. H. Park, E. Yoon and Y.-H. Kim, "Microstructural Investigation of Bilayer Growth of In- and Ga-Rich InGaN Grown by Chemical Vapor Deposition" J. Electron Mater. 38, 518 (2009)

Conference Presentations:

1. S. H. Park, J. Jang, K. Joo, D. Moon, D.-J. You, J. Park, J. Xu, Y. Nanish and E. Yoon, "Efficiency Improvement of Nonpolar a-plane GaN Light Emitting Diodes by Controlled Integration of Silica Nano-spheres", 4th International Symposium on Growth of III-Nitrides (ISGN 2012), July 16-19, 2012, St. Petersburg, Russia

2. S. H. Park, J. Jang, K. Joo, D. Moon, D.-J. You, J. Park, J. Xu, Y. Nanishi and E. Yoon, "Improved performance of a-plane GaN light emitting diodes by controlled integration of silica nano-spheres", 16th International Conference on Metal Organic Vapor Phase Epitaxy (ICMOVPE-XVI), May 20-25, 2012, Busan, Korea

3. S. H. Park, J. Park, D.-J. You, D. Moon, K.-W. Shin, J. Kim, J. Kang, Y. Nanishi and E. Yoon, "Effects of high temperature GaN nucleation layers grown with different carrier gases on a-plane GaN by metal organic chemical vapor deposition", 4th International Symposium on Advanced Plasma Science and its Applications for Nitrides and Nanomaterials (ISPlasma 2012), March 4-8, 2012, Chubu University, Aichi, Japan

4. S. H. Park, J. Park, K. Joo, D.-J. You, D. Moon, D.-U. Kim, H. Chang, S. Moon, Y.-K. Song, H. Jeon, Y. Nanishi and E. Yoon, "Improved performance of nonpolar a-plane GaN light emitting diodes by controlled integration of silica nano-spheres into GaN buffer layers", SPIE Photonics West, January 21-26, 2012, San Francisco, California, USA

5. S. H. Park, K.-H. Lee, N. H. Kim, H. J. Kim, S.-Y. Kwon, Y. H. Oh, Y.-W. Kim and E. Yoon, "Growth of Homoepitaxial GaN and In-rich InGaN/GaN Multiple Quantum Wells on Freestanding GaN Substrate by Metal-Organic Chemical Vapor Deposition", International Conference on Electronic Materials 2010 presented by International Union of Materials Research Societies (IUMRS-ICEM 2010), August 22-27, 2010, GyeonGi-Do, Korea

6. S. H. Park, S.-Y. Kwon, H. J. Kim, K.-H. Lee, N. H. Kim, M. H. Kim and E. Yoon, "Growth of In-rich InGaN/GaN Multiple Quantum Wells on freestanding GaN substrate by Metalorganic Chemical Vapor Deposition", 8th International Conference on Nitride Semiconductors (ICNS-8), October 18-23, 2009, Jeju, Korea

7. S. H. Park, H. J. Kim, S.-Y. Kwon, P. Moon, S. Choi, S.-H. Park, T. Chung, J. H. Baek and E. Yoon, "Optical Properties of Ultra-thin In-rich InGaN/GaN Multiple Quantum Well Light Emitting Diodes", SPIE Photonics West, January 19-24, 2008, San Jose, California, USA

8. S. H. Park, J. Jang, D. Moon, D.-U. Kim, H. Chang, H. Jeon, J. Xu, Y. Nanishi and E. Yoon, "Optical Polarization Properties of a-plane GaN Light Emitting Diodes by Controlled Integration of Silica Nano-spheres", 4th International Symposium on Growth of III-Nitrides (ISGN 2012), July 16-19, 2012, St. Petersburg, Russia (Accepted)

9. S. H. Park, J. Park, K. Joo, D.-J. You, D. Moon, J. Jang, D.-U. Kim, H. Chang, S. Moon, Y.-K. Song, H. Jeon, J. Xu, Y. Nanishi and E. Yoon, "Improved crystal quality of a-plane GaN on r-plane sapphire by

controlled integration of silica nano-spheres", 16th International Conference on Metal Organic Vapor Phase Epitaxy (ICMOVPE-XVI), May 20-25, 2012, Busan, Korea

10. S. H. Park, J. Park, D.-J. You, D. Moon, K. Joo, J. Kim, J. Kang, Y. Nanishi and E. Yoon, "Improved material properties of a-plane GaN on r-plane sapphire with high temperature GaN multiple buffer layers by metal-organic chemical vapor deposition", 9th International Conference on Nitride Semiconductors (ICNS-9), July 10-15, 2011, Glasgow, UK

11. S. H. Park, J. Park, D.-J. You, D. Moon, H. S. Yu, Y. Nanishi and E. Yoon, "Improved crystal quality of a-plane GaN on r-plane sapphire by controlled integration of silica nano-spheres into a-plane GaN buffer layers", 9th International Conference on Nitride Semiconductors (ICNS-9), July 10-15, 2011, Glasgow, UK

12. S. H. Park, J. Park, K. Joo, D.-J. You, S. Moon, D.-U. Kim, H. Chang, K. M. Song, Y.-K. Song, H. Jeon, Y. Nanishi and E. Yoon, "Improved output power of nonpolar a-plane GaN light emitting diodes by controlled integration of silica nano-spheres into GaN buffer layers", 9th International Conference on Nitride Semiconductors (ICNS-9), July 10-15, 2011, Glasgow, UK

13. S. H. Park, J. Park, D.-J. You, D. Moon and E. Yoon, "Improved crystal quality of a-plane GaN on r-plane sapphire with multiple buffer layers by metal-organic chemical vapor deposition", 5th Asia-Pacific Workshop on Widegap Semiconductors (APWS-2011), May 22-26, 2011, Toba, Mie, Japan

14. S. H. Park, J. Park, D. Moon, D.-J. You, J. H. Kim, J. Kim, J. Kang and E. Yoon, “Effects of r-plane sapphire substrate tilt angle on the growth behavior of nonpolar a-plane GaN”, International Workshop on Nitride Semiconductor 2010 (IWN 2010), September 19-24, 2010, Tampa FL, USA

15. S. H. Park, K.-H. Lee, N. H. Kim, J. H. Kim, D. Moon, Y. Nanishi and E. Yoon, “Growth of GaN using a GaN:C interlayer by metalorganic chemical vapor deposition”, 30th International Conference on the Physics of Semiconductors (ICPS 2010), July 25-30, 2010, Seoul, Korea

16. S. H. Park, K.-H. Lee, N. H. Kim, D. Moon, Y. Nanishi and E. Yoon, “Reduction of threading dislocation density in GaN using an GaN:C interlayer”, 2nd International Symposium on Advanced Plasma Science and its Applications for Nitrides and Nanomaterials (ISPlasma 2010), March 7-10, 2010, Nagoya, Japan

17. S. H. Park, K.-H. Lee, N. H. Kim, H. J. Kim, S.-Y. Kwon, M. H. Kim and E. Yoon, “Growth of homoepitaxial GaN and In-rich InGaN/GaN multiple quantum wells on freestanding GaN substrate by metal-organic chemical vapor deposition”, The 4th International Conference on LED and Solid State Lighting (LED 2010), February 3-5, 2010, Seoul, Korea

18. S. H. Park, S.-Y. Kwon, H. J. Kim, K.-H. Lee, N. H. Kim, M. H. Kim and E. Yoon, “Growth of In-rich InGaN/GaN multiple quantum wells on freestanding GaN substrate”, The 3rd International Conference on Display and Solid State Lighting (DSSL 2009), January 20-22, 2009,

Seoul, Korea

19. S. H. Park, H. J. Kim, S.-Y. Kwon, P. Moon, S. Choi, S.-H Park, T. Chung, J. H. Baek and E. yoon, “Internal electric field effect free characteristics of In-rich InGaN/GaN Mmultiple Qquantum well light emitting diodes”, The 2nd International Conference on Display and Solid State Lighting (DSSL 2008), January 29-31, 2008, Seoul, Korea

20. S. H. Park, H. J. Kim, S.-Y. Kwon, P. Moon, S. Choi, S.-H. Park, T. Chung, J. H. Baek, Y. S. Park and E. Yoon, “Internal electrical field effect free ultra-thin In-rich InGaN/GaN multiple quantum well light emitting diodes”, The 34th International Symposium on Compound Semiconductors (ISCS 2007), October 15-18, 2007, Kyoto, Japan

Award Events:

- Silver award at the 18th Samsung Inc. Humantech Thesis Award, Feb. 2012
- Excellent Paper award (Hynix award) as a co-author at 15th Korean Conference on Semiconductors, 2009
- Seoul Science Fellowship from Seoul Metropolitan Government, 2008~2009
- Excellent graduation thesis for bachelor's degree in Department of Materials Science and Engineering, Seoul National University, 2005